AEDC-TR-71-144

RESEARCH AND DEVELOPMENT OF A PRESSURE TRANSDUCER FOR TEST CHAMBER MEASUREMENT

O. O. Fiet

TRW Systems Group

December 1971

ARNOLD ENGINEERING DEVELOPMENT CENTER
AIR FORCE SYSTEMS COMMAND
ARNOLD AIR FORCE STATION, TENNESSEE

NOTICES

RESEARCH AND DEVELOPMENT OF A PRESSURE TRANSDUCER FOR TEST CHAMBER MEASUREMENT

O. O. Fiet

TRW Systems Group

FOREWORD

The work in this report was performed under Contract No. F40600-69-C-0009 for Arnold Engineering Development Center, Arnold Air Force Station, Tennessee 37389, by TRW Systems Group, One Space Park, Redondo Beach, California. This report includes work performed during the contract period 1 July 1969 to 30 April 1971. Report submitted 30 April 1971. The Program Element was 65701F, Project 4344, Task 37.

The work reported by the author includes the thermal analyses by N. H. Doshi given in Appendixes A and B, experimental support by C. E. Armstrong and H. E. Van Gorder, and supporting contributions by other specialists employed at TRW Systems Group.

This work was performed under the direction of Air Force Technical Manager Bruce B. Algee, Maj/CF, Directorate of Technology, Arnold Engineering Development Center, Arnold Air Force Station, Tennessee.

This technical report has been reviewed and is approved.

Maurice A. Clermont
Captain, CF
Research & Development Division
Directorate of Technology

Robert O. Dietz
Acting Director
Directorate of Technology

ABSTRACT

This report describes the initial design, construction, and development of a diaphragm type pressure balancing transducer which uses the electromagnetic "J x B" force to balance the applied fluid pressure. The pressure is measured by the direct substitution of electromagnetic pressure and a measurement of the current required to produce the balancing pressure. This technique for pressure measurement results in a direct pressure measurement by substitution and is independent of the tension and elastic constants of the pressure sensing diaphragm provided positive tension is sustained in the diaphragm. Experimental measurements on the breadboard model demonstrate the magnetic field tangential to the diaphragm should be used in calculating the restoring pressure due to diaphragm current flow. Recommendations for design improvements on the breadboard transducer are made which are intended to obtain a transducer to operate from $-195°C$ to $+250°C$. These improvements accompanied by a development effort to reduce external vibration, acoustic, and electrical disturbances (electronic system and installation practices) are expected to enable demonstration of pressure measurements to 10^{-8} torr using adaptations of available commercial laboratory equipment. The development of this type of pressure transducer is important for orbital rocket engine test chamber pressure measurements because it will enable fundamental direct physical pressure measurement (force per unit area) at low pressures independent of gas species. Results projected from experimental work completed on the breadboard model confirm earlier predictions that the performance goals for a temperature range of $-195°C$ to $+250°C$ and sensitivity to 10^{-8} torr may be obtained.

TABLE OF CONTENTS

ILLUSTRATIONS

TABLES

I

INTRODUCTION

Present and future tests scheduled at the Arnold Engineering Development Center, Arnold Air Force Station, Tullahoma, Tennessee (AEDC), on rocket exhaust plume studies in deep space and orbital pressure environments require an accurate measurement of test chamber pressures to 10^{-8} torr independent of gas species present. The pressure measurement should be measured by a sensor whose response is a direct response of the fundamental definition of pressure (normal fluid force per unit area). Several good electromechanical transducers utilizing diaphragms or Bourdon helixes are available for direct pressure measurement which do not have the desired pressure sensitivity and stability for a wide transducer operating temperature (cryogenic to 300°C). Available electromechanical transducers do not provide a direct closed-loop substitution calibration and measurement. Available ion gauges can measure the desired pressure range with limited accuracy but their calibration is species dependent. Commercial gauges are not available to make the desired pressure measurement independent of species to 10^{-8} torr.

This report describes the initial effort to develop an accurate pressure gauge to measure pressure from 1 torr to 10^{-8} torr independent of species. The transducer is essentially a taut diaphragm transducer whose applied fluid pressure component is opposed by an identical electromagnetic pressure on the diaphragm. The current or voltage required for the opposing electromagnetic pressure is measured and thus provides a direct substitution measurement of the applied fluid pressure. The generation of the opposing electromagnetic pressure is provided by a self-balancing high gain electronic control system.

A self-balancing pressure transducer has been constructed and experimental system performance evaluations have been made. The results of this work are the basis for modifications which are required to approach the desired performance objectives. The work performed included the following:

   a. Design of a breadboard transducer.

   b. Construction of the breadboard transducer.

   c. Evaluation of the breadboard transducer using standard laboratory equipment with a minimum of custom constructed adaptive equipment.

   d. Preliminary design of a coordinated electronic system for use with the transducer.

   e. A final report on all work done under the contract with an analysis of the results and recommendations for the design and manufacture of the equipment required for a space chamber facility.

   f. The breadboard transducer was delivered to AEDC with this final report.

The objective of this research program is to develop a pressure transducer suitable for the orbital test chamber application to measure pressure from 1 torr to 10^{-8} torr with high pressure response speed of 50 milliseconds or better and an operational range from cryogenics to 300°C.

.

II

SUMMARY

A diaphragm pressure transducer may be constructed utilizing a circular diaphragm of uniform thickness with a differential fluid pressure applied to opposite faces of the diaphragm. The deflection of a taut diaphragm will be proportional to the applied differential pressure for small differntial pressures and hence a measurement of diaphragm deflection by suitable electronic means (inductance variation, photo position sensor, capcitance variation, oscillating wave reflection interference measurement) can provide an open loop electrical transduction for measurement of the applied fluid pressure. Successful transducers of this type·are commercially available but they are limited to higher pressure measurements and closely controlled environmental conditions. Their response speed is also limited by methods used for local control of the transducer environment and the fluid pressure connections.

The performance of the open loop taut diaphragm pressure transducer is limited by the following conditions. The deflection of the diaphragm by applied fluid pressure is dependent upon the elastic properties of the diaphragm which are dependent upon temperature, gas environment, corrosion, previous mechanical flexure history, initial tension, fatigue and creep. These problems are minimized by careful mechanical design and operation of the transducer within a constant temperature electrically controlled enclosure. The fluid connections for pressure measurements are also constricted to minimize external environmental effects, thus restricting the attainable fluid response speed at the transducer diaphragm relative to the applied pressure function.

Available sensitive diaphragm differential pressure gauges operate "open loop" and are therefore limited in accuracy and sensitivity by the elastic and temperature sensitive characteristics of the diaphragm assembly. The differential pressure meter described in this report measures pressure by a direct and identical substitution of an opposing electromagnetic pressure on a diaphragm sensor element. Insensitivity to environmental effects is obtained by use of a closed-loop servo substituting an idential electromagnetic pressure.

The electromagnetic pressure used as a null position restoring pressure for the diaphragm may be obtained by using an electric field normal to the diaphragm boundary or a transverse control current and an orthogonal constant bias magnetic field parallel to the diaphragm surface or a combination of electric and magnetic fields. The transverse control current and steady magnetic field were selected because an electric field normal to the boundary can ionize low pressure gases disabling the electric field control function.

The fundamental functioning of the transverse current and magnetic field pressure transducer is illustrated in Figure 1. The equation given is consistent with the rational MKS system of units where

$$J_s = Jt^{(1)}$$
<div align="right">Eq. (1)</div>

3

and

t = Diaphragm thickness in meters

J = Current density in amperes per square meter

J_s = Current sheet density in amperes per meter

① CURRENT SHEET DIAPHRAGM
② MOUNTING BLOCK & CURRENT RETURN
③ ELECTICAL INSULATION
④ CURRENT RETURN CONNECTION
⑤ CURRENT INPUT CONNECTION

$\bar{B}$ = APPLIED EXTERNAL UNIFORM TRANSVERSE MAGNETIC FIELD
$\bar{J}_S$ = EQUIVALENT SURFACE CURRENT INTENSITY
$\bar{P}_{IB}$ = MAGNETIC PRESSURE ON CURRENT SHEET

$$\bar{P}_{IB} = \bar{J}_S \times \bar{B}$$
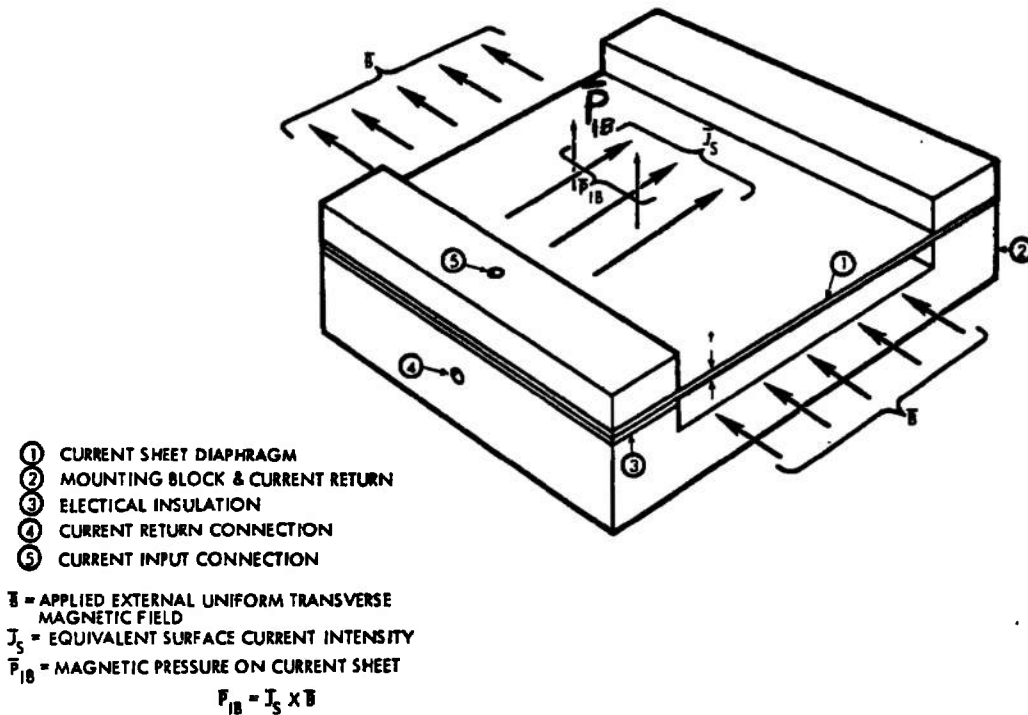
Figure 1. . Basic Current Sheet Pressure Transducer

The current sheet density J_s is controlled by an electrical control system to exactly oppose the applied fluid pressure. The steady magnetic bias $\bar{B}$ is supplied by a permanent magnet and the current sheet current is supplied by a diaphragm position error control amplifier.

A pressure balancing diaphragm pressure transducer was constructed as part of the research effort utilizing the $\bar{J}_s \times \bar{B}$ pressure normal to the diaphragm boundary to counterbalance the applied fluid pressure. Important design considerations pertinent to this application included (1) selection of assembly materials for the transducer assembly to assure minimum thermal stress for a wide temperature range; (2) a practical diaphragm tensioning method which would assure the diaphragm is in tension but not overstressed for a wide range of operating temperatures; and (3) selection of a diaphragm material with the desired matching mechanical and thermal properties which also had low electrical resistivity for low electrical heating during the flow of the necessary position restoring control current. A high magnetic permeability and saturation flux density was also desired.

to obtain a high restoring pressure conversion efficiency. Excessive diaphragm current density and resistivity will heat the central portion of the diaphragm resulting in linear expansion and diaphragm buckling when the expansion is sufficient to produce a negative tension in the exposed portion of the diaphragm. Thermal buckling of the diaphragm will disable the null position sensor function and, consequently, the pressure balancing system is disabled.

Experimental results obtained with the breadboard transducer indicate the high magnetic saturation and permeability properties of the selected diaphragm material are not effective in obtaining the predicted enhanced current sheet deflection sensitivity. The sensitivity was less than computed on the basis of computed diaphragm flux density by a factor of thirty; this factor is identical to the ratio of the computed diaphragm flux density to the tangential flux density external to the diaphragm, hence it is concluded that the current sheet magnetic permeability does not enhance the current deflection sensitivity. For this reason a nonmagnetic diaphragm material with very low electrical resistivity and youngs modulus with appropriate matching thermal and mechanical properties may produce better performance than the magnetic diaphragm material used in the breadboard. The predicted performance improvement for equal heating of a corresponding silver diaphragm is 2.61 times. This performance improvement can be directly confirmed by substituting a silver diaphragm in the present transducer assembly. The transducer assembly may be modified to concentrate the available permanent magnet magnetizing force and flux within the useful working area of the diaphragm to obtain a calculated increase in current deflection sensitivity of 1.455 times. The substitution of the silver diaphragm which is nonmagnetic cannot increase the diaphragm magnetic flux density by making a direct magnetic connection to the magnet pole faces, hence a reduction in the width of the silver diaphragm to a width just sufficient for clamping the active area will reduce the restoring pressure current by the ratio of diaphragm widths transverse to the current flow direction. This will improve the current deflection sensitivity by 1.12 times with the existing clamp assembly. The calculated effect of the three improvements considered here is 4.26 times. Two of the improvements can be obtained by substitution of a suitable width silver diaphragm in the present frame assembly to obtain an improvement of 2.92 times.

The application of a pressure transducer for orbital test chamber pressure measurements requires the development of a suitable transducer for very low pressure measurements, hence a current deflection sensitivity less than first predicted can perform well for lower pressure measurements up to say .1 torr instead of 1 torr. Other performance factors are also affected by lower current deflection sensitivity. The transducer gain (loss) from current input to the diaphragm deflection sensor output is reduced in direct proportion to the current deflection sensitivity. This gain reduction can be offset by a corresponding increase in the diaphragm position sensor supply voltage. This increase is limited by increasing electric field forces on the diaphragm which interact with the desired pressure substitution measurement function. The increased electric field can also permit ionization at low residual gas pressures, thus disabling the transducer, hence an optimum choice of position sensor supply voltage and current deflection sensitivity is required.

An increased transducer loss from the current input to the diaphragm position sensor output causes a proportional reduction in output signal from the transducer relative to ambient electrical and pressure noise. More design and development effort is therefore required to minimize the electrical and pressure noise disturbances.

Standard laboratory equipment has been adapted to perform the necessary electronic control and display functions required by the transducers. A detailed description of the custom built adaptive accessories and on the operation and tests performed are given.

The breadboard transducer which was designed, constructed and tested is documented by preliminary drawings. The commercial use of the design is defined[2]. Improvements obtained during this contract are described, and a plan for continued development and completion of the transducer and coordinated electronic system is given.

An experimental pressure sensitivity of 1.56 torr per volt output was measured with the breadboard transducer. This would result in a realizeable ultimate sensitivity with the available laboratory equipment of 1.56 x 10^{-9} torr full scale on the 10^{-9} volt range of the amplifier used. Demonstration of this ultimate sensitivity will require improvement of the transducer installation and test connections to reduce the external disturbances caused by vibration, acoustic and electrical noise.

The design improvement study supporting the recommended breadboard construction changes indicate a modified transducer construced of available materials may operate over a temperature range of -195°C to +250°C.

Completion of the transducer improvements and associated installation and electronic system development is recommended to demonstrate performance to 10^{-8} torr over a wide ambient temperature range before design and construction of the final orbital test chamber hardware is undertaken.

III

TRANSDUCER DESIGN

3.1 TRANSDUCER CONCEPT AND CONSTRUCTION

The initial design concepts for the pressure balancing transducer described in this report are delineated in earlier documents.[2,3] The transducer illustrated utilized a bifilar diaphragm and frame assembly similar to the breadboard model constructed here. The diaphragm assembly was centered within a circular cylinder magnet assembly with magnet poles on diametrically opposing cylindrical boundaries. The magnetic poles were connected magnetically to opposite edges of the rectangular magnetic current sheet diaphragms by magnetic pole shoes. The current control connections to the diaphragm were made on the orthogonal edges of the rectangular diaphragm by heavy constant potential bus bar connections. The diaphragm magnetic connections are also made to the diaphragm by heavy rectangular high permeability magnet pole shoes to assure a constant magnetic potential at each edge of the diaphragm and consequently a constant and uniform magnetic flux density within the diaphragm.[1]

The constant thickness, rectangular, homogeneous resistivity and permeability diaphragm, provide the necessary boundary conditions to enforce the desired uniform current and flux density throughout the diaphragm.[1] This is essential to obtain a uniform and constant distribution of the electromagnetic pressure balancing force on the working area of the diaphragm.

The breadboard transducer used for this work is a similar configuration to the earlier description except for the magnet arrangement and connections which provide improved uniformity of magnetic flux in and near the diaphragm. Figure 2 illustrates an exterior of the breadboard transducer and Figure 3 provides an interior view of the reference pressure chamber and flange connection. Figure 4 shows construction details of the breadboard transducer. Table I is a list of the transducer assembly components.

3.1.1 The Current Sheet Pressure Balancing Meter

Figure 5 is a block diagram of the proposed diaphragm type differential pressure meter system incorporating features described here. An electromechanical closed loop null seeking servo system is used. The pressure sensing and feedback error functions are accomplished by a common diaphragm. The electrical capacity of this diaphragm is compared to the electrical capacity of an identical reference diaphragm. The capacity change which is proportional to the applied differential fluid pressure on the pressure sensor diaphragm is converted to electrical output by a capacity bridge circuit. The AC output of the bridge circuit is amplified by a narrow band, low noise AC amplifier and is detected by a synchronous AC

---

[1]Ref. cited pg. 137, pg. 249.
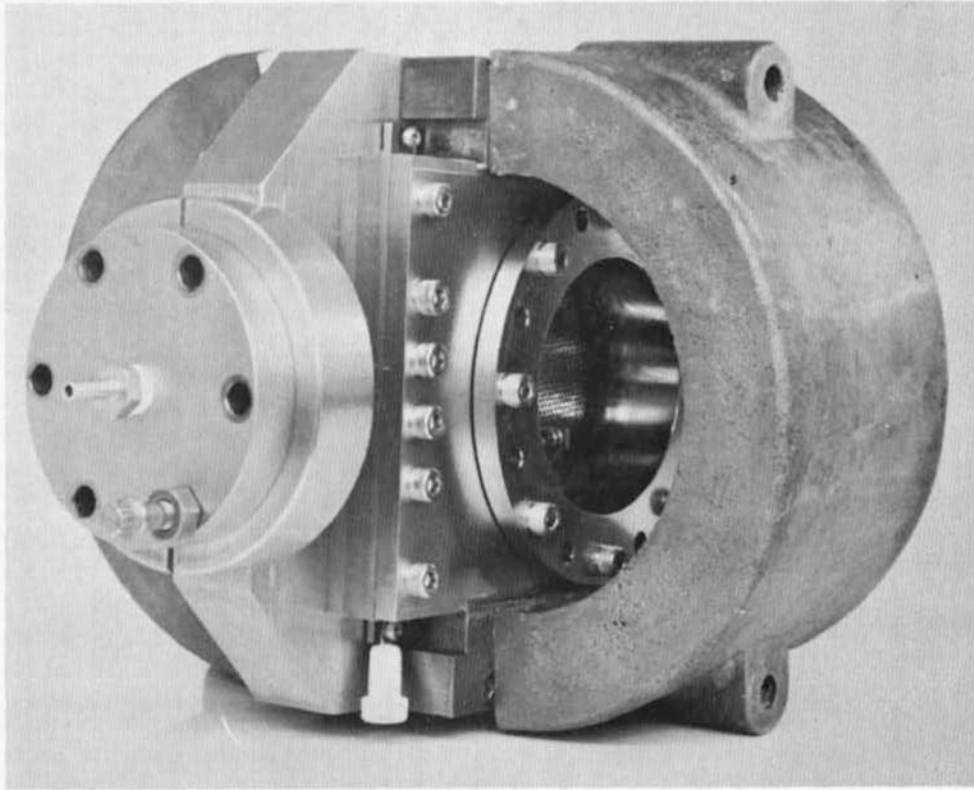
Figure 2. Exterior View of Breadboard Transducer.
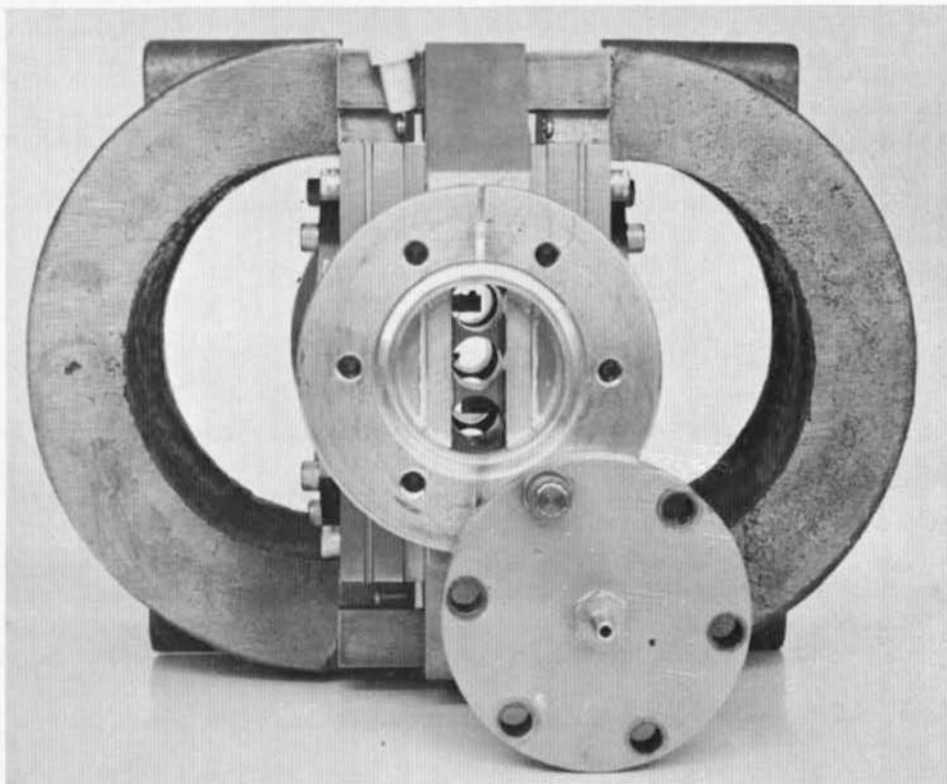
Figure 3. Breadboard Transducer Showing Reference Pressure Chamber.

STRIP SPACER
SK4726-70-20
4 PLACES

BUSS BAR
SK4726-70-18
4 PLACES

SK4726-71-29

NUT 5/16-18
ROD THREADED 5/16-18 x
6 0 LG (CARPENTER NO. 10
OR EQUIVALENT

MAGNET
PERMAG CORP
P/N S-130

FRAME ASSY
SK4726-70-6

DIAPHRAGM PLATE ASSY
SK4726-70-14

RING, TENSIONING
SK4726-70-22

PLATE ASSY
SK4726-70-11

SCREW 10-32 x 5LG
24 PLACES

SCREW 10-32 x 1 0LG
16 PLACES

CARPENTER
NO 10 OR EQUIV

CONNECTOR

FLANGE-CONNECTOR
SK4726-70-24

Figure 4. Breadboard Transducer Assembly.

9

AEDC-TR-71-144

TABLE I

TRANSDUCER ASSEMBLY COMPONENTS

No. Req.	Drawing No.	Title
1	SK4726-71-29	Final Assembly
1	SK4726-70-5	Ultra-Vac Assembly
1	SK4726-70-6	Frame Assembly
1	SK4726-70-7	Frame Assembly (Brazement)
1	SK4726-70-8	Frame
2	SK4726-70-9	Flange
2	SK4726-70-10	Plate Assembly Backup
2	SK4726-70-11	Plate Assembly (Welded)
2	SK4726-70-12	Ring
2	SK4726-70-13	Pole
2	SK4726-70-14	Diaphragm Plate Assembly
2	SK4726-70-15	End Plate
2	SK4726-70-16	Top Plate
2	SK4726-70-17	Bottom Plate
2	SK4726-70-18	Buss Bar
2	SK4726-70-19	Insulator
4(-1), 4(-2)	SK4726-70-20	Spacer
24	10-32 x .5 Lg	Screws Socket Head*
16	10-32 x 1.0 Lg	Screws Socket Head*
2	5/16-18 x 6.0 Lg	Rod, Threaded*
4	5/16-18	Nuts*
2	Permag Corp. P/N S-130	Magnet

*Carpenter No. 10 or equivalent.

10

PRESSURE SENSOR CAPACITOR
AND CONTROL DIAPHRAGM

PRESSURE SENSOR CAPACITOR ELECTRODE

REFERENCE PRESSURE SENSOR
CAPACITOR ELECTRODE

STABLE D.C.
POWER SUPPLY

PRESSURE
SIGNAL

VOLTAGE CONTROLLED
REFERENCE OSCILLATOR

VCO CONTROL INPUT

f_o

f_o

REFERENCE AND
COMPENSATING
CAPACITOR
DIAPHRAGM

DECADE
PRESSURE
DIFFERENTIAL
SETTING

NARROW
BAND
FILTER

AC
NARROW BAND
AMPLIFIER VOLTAGE
GAIN $\geq 10^8$ NOISE
FIGURE $\cong$ 3DB

SYNCHRONUS
DETECTOR

PHASE ERROR
SIGNAL

PRESSURE ERROR
SIGNAL

D.C. ERROR
AMPLIFIER
CONTROL

PRESSURE SIGNAL

ANALOG OR
DIGITAL
PRESSURE
DISPLAY

PRESSURE RECORDER

Figure 5. Pressure Balancing Meter System.

demodulator. Two DC outputs are obtained from the synchronous demodulator output. One is proportional to the applied fluid differential pressure. The second output is proportional to phase error at the amplifier output. The phase error voltage is used to tune the capacitance bridge supply oscillator to a frequency producing zero phase error. This assures operation of the oscillator at the frequency where the error amplifier gain and signal to noise ratio are maximum. The restoring pressure is applied to the pressure sensor diaphragm by a low frequency and/or DC current which is an amplified output of the pressure error signal. Essentially, no direct signal coupling exists between the low frequency and DC current restoring force and the high frequency AC pressure sensing voltages on the pressure sensor diaphragm because of carrier frequency selection and frequency separation filters.

3.1.2 Theoretical Performance

The current sheet type of fluid pressure transducer is illustrated in Figures 1 to 4. It is necessary to utilize a solid conducting boundary to provide a direct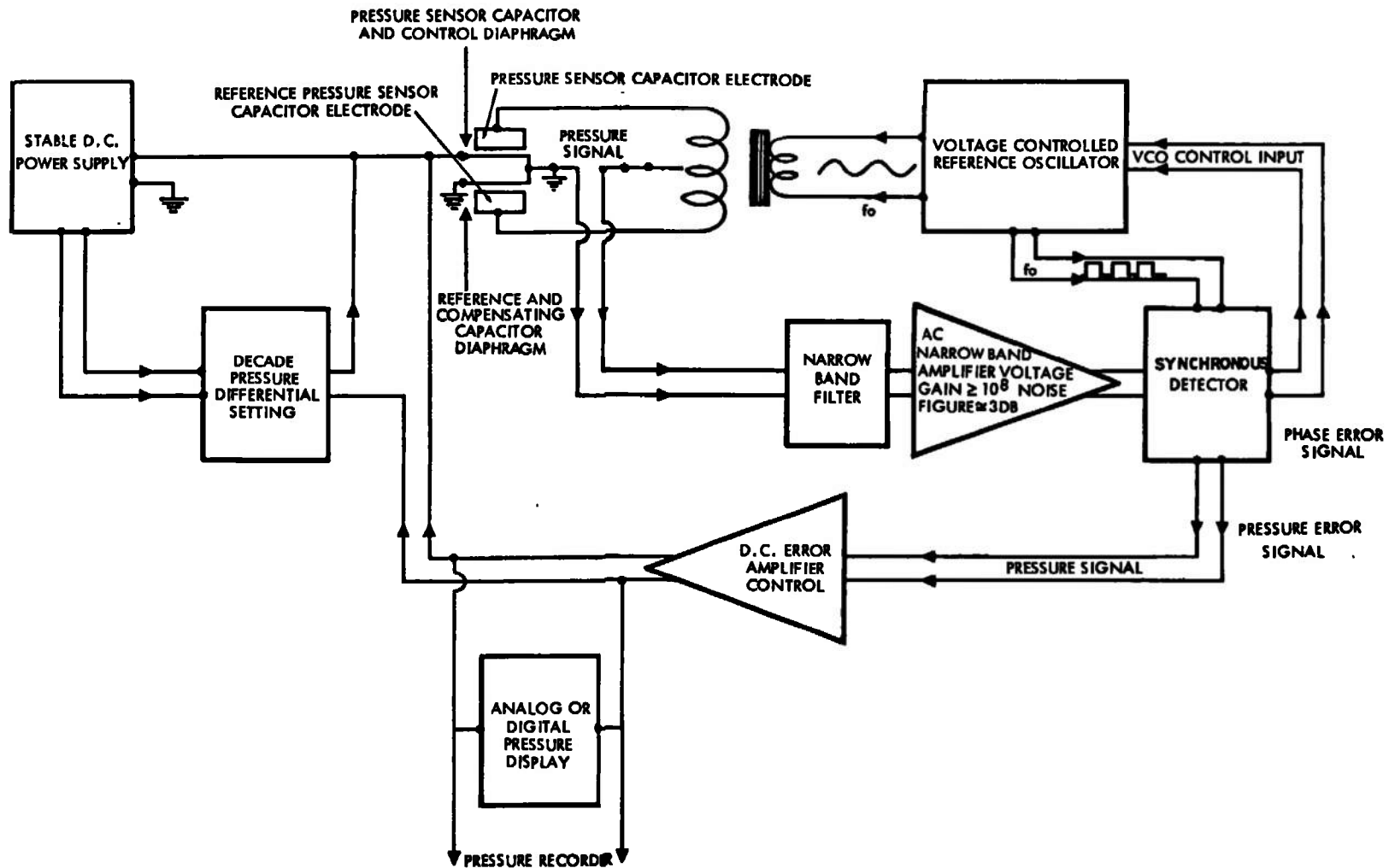 and opposing coupling of the pressure due to electromagnetic force and the fluid pressure. The static fluid pressure against a fixed position solid boundary surface is uniform and normal to the boundary surface, hence, an identical substitution of electromagnetic pressure must be uniform and normal to the exposed boundary surface. A current flowing in a uniform homogeneous conducting sheet in a tangential magnetic field transverse to the direction of current flow will have a constant normal magnetic pressure at all points where the cross product of the current density and the magnetic field intensity is maintained constant. Hence, the current sheet can meet the fluid pressure identity requirement at the solid current sheet boundary.

The magnetic force density applied at a point in a solid current conductor is given by Equation 2, in rational MKS units

$$\overline{F}_m = \overline{J} \times \overline{B} \qquad \qquad \text{Eq (2)}$$

where: $\overline{F}_m$ = magnetic force density, Newtons/cubic meter

$\overline{J}$ = current density, amperes/square meter

$\overline{B}$ = magnetic flux density, Webers/square meter

The bar identifies the vector quantity.

M.K.S. units will be used for illustrative electromagnetic calculations.

A current sheet diaphragm with only an x component of current and a y component of magnetic field will have only a z component of force.

$$F_{mz} = J_x B_y \qquad \qquad \text{Eq (3)}$$

The magnetic force density at all operating points within the current sheet may be integrated to obtain the pressure at any point normal to the current sheet/dielectric interface and the resulting force per unit area, P_{mz} is:

$$\frac{\iint F_{mz} \, dt \, dA}{\int dA} = \frac{\int_0^1 \int_0^w \int_0^t J_x \, B_y \cdot dx \, dy \, dz}{\int_0^1 \int_0^w dx \, dy} = P_{mz} \qquad \text{Eq (4)}$$

If $J_x B_y$ is constant within the working boundaries of the diaphragm, 1, w and t, the magnetic force density, F_{mz}, and boundary pressure, P_{mz}, are constant.

$$P_{mz} = (J_x t) \, B_y = \frac{I}{w} \, B_y \qquad \text{Eq (5)}$$

where: A = area of diaphragm surface, square meters

P_{mz} = magnetic pressure normal to diaphragm surface, Newtons/ square meter

I = current in working diaphragm, amperes

w = width of working diaphragm transverse to current flow, meters

1 = length of working diaphragm, meters

t = thickness of working diaphragm, meters

$\overline{F}_m$ = average force density at any point in the working diaphragm

B_y = y component of magnetic flux density

A uniform dc current density is obtained in the working portion of the pressure sensing diaphragm by making the current sheet cross section transverse to the current flow of constant thickness and width (constant current conducting channel cross section). External connections are made to heavy rectangular connecting blocks perpendicular to the direction of current flow at each end of the current sheet. The current sheet material has a homogeneous, isotropic conductivity and obeys Ohm's law.

$$\overline{J} = g \, \overline{E} \qquad \text{Eq (6)}$$

$$J_x = g \, E_x \qquad \text{Eq (7)}$$

3.1.3 Performance of Iron Diaphragm

Consider a current sheet transducer with the following characteristics:

Diaphragm material = .0005 inch thick hydrogen annealed pure iron
Diameter of working diaphragm = 2.645 inch
Saturation induction = 20,000 Gauss = 2 Webers/square meter
Resistivity = 10 x 10^{-6} ohm cm = 10^{-7} ohm meters
Ultimate strength (annealed) = 42,000 psi
Yield strength (annealed) = 19,000 psi
Modulus of elasticity = 29.8 x 10^6 psi
Relative permeability @ 20,000 Gauss $\simeq$ 100
Specific gravity = 7.88
Coefficient of linear thermal expansion (20-100°C) = 12.25 x 10^{-6}/°C

Electromagnetic calculations are in M.K.S. units

B_y = Constant transverse magnetic flux density in diaphragm = 2 Webers/m². One atmosphere pressure is 14.7 psia or 760 mm of Hg, the equivalent pressure, P_{za} in Newtons/m² is

$$P_{za} = \frac{14.7 \ (39.37)^2}{.224} = 1.02 \times 10^5 \ \text{Newtons/m}^2\text{/atmosphere}$$

The equivalent uniform surface current density, per meter diaphragm width, $J_x t$, is

$$J_x t = \frac{P_z}{B_y} \ \text{amperes/meter} \qquad\qquad \text{Eq (8)}$$

The surface current density, for one atmosphere differential pressure, P_{za}, is $J_{xa} t$,

$$J_{xz} t = \frac{P_{za}}{B_y} = \frac{1.02 \times 10^5}{2} = 5.1 \times 10^4 \ \text{amperes/meter/atmosphere}$$

The surface current density, $J_{xmm} t$, for 1 mm Hg differential pressure is

$$J_{xmm} t = \frac{5.1 \times 10^4}{760} = 67.2 \ \text{amperes/meter/mm Hg}$$

The corresponding surface current densities in amperes per inch width are

$$J''_{xa} t = \frac{5.1 \times 10^4}{39.37} = 1.29 \times 10^3 \ \text{amperes/inch/atmosphere}$$

and

$$J''_{xa} t = \frac{67.2}{39.37} = 1.708 \ \text{amperes/inch/mm Hg}$$

This current is readily supplied by a transistor circuit for practical diaphragm widths.

3.1.4 Magnetic Flux Densities at the Diaphragm

Measurements were made on the breadboard transducer to check the computed current deflection sensitivity based on a diaphragm magnetic flux density of 2 Webers/square meter. The measurement of current deflection sensitivity observed in the lab was 30.2 times less than the current deflection sensitivity computed above; i.e.:

$$J''_{xa} = 1.708 \ \text{amperes/inch/mm Hg (calculated)}$$

$$J''_{xa} = 51.5 \ \text{amperes/inch/mm Hg (measured)}$$

$$\frac{J''_{xa} \ \text{measured}}{J''_{xa} \ \text{calculated}} = \frac{51.5}{1.708} = 30.2 \ \text{times}$$

This discrepancy between theory and measurement was not readily explained, consequently a detailed laboratory investigation was made to establish a reason for the discrepancy.

The tangential magnetic flux density was measured near the diaphragm with a RFL Model 505 gaussmeter at the locations given in Table II. These measurements were made with a long-handled hall probe, the frame and magnets interfered with the optimum probe positioning for maximum flux density readings at locations close to the diaphragm surface; consequently, the tabulated flux densities are slightly less than the actual flux density because of probe misalignment. The diaphragm and frame clamping assembly was removed and soft iron pole shoes were placed on the magnets. The flux densities measured for this case in the plane of the diaphragm are tabulated in Table III. The flux densities tabulated in Tables II and III indicate a uniform tangential flux density is closely realized in the breadboard transducer. Probe positioning was by visual location without scales or gauges using a hand-held probe. A precision mechanical positioning device would improve the uniformity of measured flux densities.

The measured tangential flux density with the diaphragm installed can be used to compute the magnetic flux density in the diaphragm by reference to a normal magnetization curve for the diaphragm material.[4] This curve is given in C.G.S. units. A tangential flux density of 650 Gauss corresponds to a magnetizing force of 650 Oersteds in C.G.S. units; hence, by reference to Figure 4-30 of Reference 4, we find the intrinsic flux density, Bi, for annealed magnetic ingot iron to be:

$$Bi = 20.7 \text{ Kilogauss}$$

The corresponding total flux density in the diaphragm is:[4]

$$B = Bi + H \qquad\qquad \text{Eq (9)}$$

$$B = 20.7 + .650 = 21.350 \text{ Kilogauss}$$

This measurement confirms the design goal of B = 20 Kilogauss is satisfied with a 6 percent margin of safety.

3.1.5 Diaphragm Heating Due to Current

The current flow in the transducer diaphragm produces Joule heating proportional to the electrical resistivity and the square of the pressure balancing current density. The electrical heating dissipation density in the diaphragm is:

$$\frac{(W_R)}{V} = \rho J^2 \qquad\qquad \text{Eq (10)}$$

Ref. 4, Figure 4-30, pg. 152, Ref. 4, pg. 25.

TABLE II

MEASURED DIAPHRAGM TANGENTIAL FLUX DENSITY

Working Aperture Location	Connector Side Gauss Top Diaphragm	Gauss Bottom Diaphragm
Left Side	640	640
Right Side	650	640
Upper Side	600	590
Lower Side	600	600
Center	610	610

TABLE III

MEASURED FLUX DENSITIES IN DIAPHRAGM PLANE

(Diaphragm Removed)

Location	Gauss
Left and Right Pole Center	700
Diaphragm Center	620
Diaphragm Edge Midway Between Poles	600
Diaphragm Edge at Poles	700
Diaphragm Edge at 1/4 Distance Between Poles	640

where: V = volume of working current sheet, cubic meters

W_R = power dissipation due to current flow, watts, or Joules/second

ρ = resistivity of current sheet, Ohm meters

The surface dissipation density $W_R/2A$ in watts/square meter considering both outer surfaces of the diaphragm is:

$$\frac{W_R}{2A} = \frac{\rho t}{2} \quad J^2 = \frac{\rho}{2t} (tJ)^2 = \frac{\rho}{2t} \left(\frac{I}{W}\right)^2 \qquad \text{Eq (11)}$$

where: A = diaphragm area, in square meters

For a pure annealed iron diaphragm with a magnetic restoring pressure ΔP_m = 1 mm Hg, the surface heat dissipation is, for $\rho = 10^{-7}$ ohm meters:

The original computed design current sheet current density, $J_s = Jt$, for 1 mm Hg ΔP and B = 2 Webers/m^2 is 67.2 amperes/meter.

The breadboard model current sheet thickness is:

$$t_z = 5 \times 10^{-4} \text{ inches} = 1.27 \times 10^{-5} \text{ meters}$$

$$\frac{W_R}{2A} = \frac{10^{-7} (67.2)^2}{2 (1.27) \times 10^{-5}} = 17.75 \text{ watts/square meter}$$

$$\frac{W_R}{2A} = \frac{17.75}{(39.37)^2} = 1.143 \times 10^{-2} \text{ watts/square inch}$$

The 11.4 milliwatts/square inch of diaphragm Joule heating can be dissipated by radiation and/or conduction without excessive temperature rise. Proper assembly of the diaphragm in the frame will assure sufficient initial tension to prevent buckling of the central diaphragm area due to thermal expansion. The diaphragm heat dissipation calculation is based on the design premises assumed for the breadboard transducer, i.e., a pure annealed iron diaphragm 5 x 10^{-4} inches thick with a current sheet density of 67.2 amperes/meter. This current sheet density was computed for 1 mm Hg restoring pressure and a diaphragm flux density of 2 Webers/m^2. It was believed that the flux density in the diaphragm rather than tangential to it is effective in producing the electromagnetic pressure given by Equation 5. The laboratory investigation on the breadboard model has shown the tangential magnetic flux density should be used in Equation 5 to compute the electromagnetic pressure.

The diaphragm Joule heating for 1 mm Hg ΔP based on the experimentally determined diaphragm tangential flux density which should be used in the electromagnetic pressure Equation 5 will be calculated for the following readjusted design parameters. These design parameters will permit direct substitution of a new and improved diaphragm in the existing breadboard

model transducer without extensive modification. The recommended new design parameters are:

Tangential flux density (measured on breadboard model) = 650 gauss

Diaphragm thickness = 5×10^{-4} inches

The physical constants for a silver diaphragm are:

Density = .379 lbs/cu in

Linear thermal expansion = $10.9 \times 10^{-6}/°F = 19.6 \times 10^{-6}/°C$

Thermal conductivity = 242 BTU/hr/sq ft/°F/ft

Specific heat = .056 BTU/lb/°F

Electrical resistivity = 1.47×10^{-6} ohm cm = 1.47×10^{-8} ohm meters

Modulus of elasticity 11×10^6 psi

Tensile strength 25×10^3 psi

Yield strength (.2 percent offset) 12×10^3 psi

Elongation (percent in 2 inches) 48 percent

The adjusted current sheet density for a change of magnetic flux density from 2 Webers/1 sq. m. to .065 Webers/sq. m. and 1 mm Hg electromagnetic pressure is:

$$\frac{I_x}{W_y} = t_z J_x = \frac{67.2 \ (2)}{.065} = 2065 \text{ amperes/meter/mm Hg}$$

The Joule heating for the silver diaphragm at 1 mm Hg electromagnetic pressure (2065 amperes/meter) is from Equation 11.

$$\frac{W_R}{2A} = \frac{\rho}{2t} \ (\frac{I}{W})^2 = \frac{1.47 \times 10^{-8} \ (2.065 \times 10^3)^2}{2 \ (1.27) \times 10^{-5}} =$$

$$= 2.47 \times 10^3 \text{ watts/square meter at 1 mm } \Delta P$$

The Joule heating for 1 mm ΔP is approximately 100 times the original breadboard design value. This may require a decrease of maximum full scale pressure range to .1 mm ΔP under some adverse environmental operating conditions. The redesigned dissipation density at .1 mm ΔP is

$$\frac{W_R}{2A} = 24.7 \text{ watts/m}^2 \text{ at .1 mm } \Delta P$$

This dissipation density is approximately equal to the original breadboard design dissipation of 17.7 watts/m^2.

3.1.6 Other Temperature Effects

The heating caused by the restoring force current flow is one of the temperature disturbances which may affect the pressure balancing gauge

system performance. A summary of possible temperature disturbances are:

1. Heating caused by diaphragm position restoring current.

2. Transient and differential temperature effects caused by external gas temperature and radiant exposure.

3. Initial starting temperature stabilization transients of the transducer temperature controller.

The diaphragm heating caused by restoring current flow will not produce a ΔP readout error for transient or steady state ΔP changes if sufficient initial diaphragm tension is used.

The degree of prestressing required for diaphragm Joule heating can be determined if the maximum temperature difference between the diaphragm and the frame is known. For mercury vapor at one torr pressure, a typical temperature difference $\Delta T = 1.2^\circ C$ was computed. (Appendix A).

The stress decrease per degree centigrade in the iron diaphragm due to Joule heating only is obtained as follows:[9]

For pure iron

ΔS = stress decrease in psi

E = 30 x 10^6 psi, Young's Modulus for pure iron

ν = 0.3, Poisson's Ratio

ΔT = $1.0^\circ C$ temperature difference

α = 1.22 x 10^{-5} linear expansion coefficient for pure iron

$$\Delta S = \frac{\Delta T \alpha E}{(1-\nu)} \qquad \text{Eq (12)}$$

$$\Delta S = \frac{1.22 \times 10^{-5} \times 30 \times 10^6}{(1 - 0.30)} = 533 \text{ PSI/}^\circ C \text{ rise for pure iron}$$

Likewise the stress decrease for a silver diaphragm with $1^\circ C$ Joule heating is:

For silver

E = 11 x 10^6 PSI Young's Modulus

ν $\approx$ .3, Poisson's Ratio

ΔT = $1^\circ C$

α = 19.6 x $10^{-6}/^\circ C$ linear expansion coefficient

$$\Delta S = \frac{(1^\circ) \ 19.6 \times 10^{-6} \times 11 \times 10^6}{.7} = 308 \text{ PSI}$$

Reference 9, pg. 335.

If the silver diaphragm was pre-stressed to 10,000 PSI the maximum diaphragm temperature rise permissible without buckling would be:

$$\Delta T_{max} = \frac{\Delta S_{max} (1-\nu)}{\alpha E} \qquad \text{Eq (13)}$$

The maximum temperature rise for a silver diaphragm would be:

$$\Delta T_{max} = \frac{10^4 \, (.7)}{19.6 \times 10^{-6} \times 11 \times 10^6} = 32.4^\circ C$$

3.1.7 Thermal Stress Due to Temperature Change

The diaphragm clamping frame and the diaphragm are made of different materials which may have different linear coefficients of thermal expansion. If this is true, a thermal stress change will develop in the diaphragm when the frame and diaphragm temperature change an equal amount. This problem is solved in a manner similar to the diaphragm temperature rise problem except the difference in linear expansion coefficient between the frame and diaphragm material is used for calculation of the stress change. The choice of matching temperature coefficient materials for the diaphragm and frame can be a difficult problem when economical fabrication of a small quantity of transducers is required for the following reasons:

1. The diaphragm and frame materials must be available at reasonable prices, short delivery time and in the quantity required.

2. Both materials must satisfy the mechanical, electrical and physical requirements to an acceptable degree.

In the case of the breadboard transducer constructed for this project, an extensive investigation was made to find a suitable frame material which would closely match the linear expansion coefficient of the pure iron diaphragm material and satisfy the non-magnetic and fabrication requirements. A very close match is difficult because of insufficient and conflicting published data on both materials over the desired operating temperature range. AISI stainless steel alloy No. 310 was selected for the frame as the best available temperature coefficient match, good vacuum properties, satisfactory fabrication characteristics, and very low magnetic permeability after cold working. The differential expansion coefficient, $\Delta\alpha$, between pure iron and AISI-310 was estimated to be 1 to 1.5 x 10^{-6}/$^\circ$F from various sources.[14,15,16,17,18]

For the case of a differential expansion coefficient, $\Delta\alpha$, between the frame and diaphragm:

$$\Delta S = \frac{\Delta T \Delta \alpha E}{(1-\nu)} \qquad \text{Eq (14)}$$

and

$$\Delta T = \frac{\Delta S \, (1-\nu)}{\Delta \alpha E} \qquad \text{Eq (15)}$$

For a pure iron diaphragm

S = 27,000 PSI yield stress

Operating Stress S_{max} = 13,500 PSI at room temperature

$\sim 68^{o}F = 20^{o}C$

Assume $\Delta\alpha$ 1 x 10^{-6} parts/^{o}F

The α of AISI-310 is always larger than the α of pure iron
by 1 to 1.5 x $10^{-6}/^{o}F$

For decreasing temperature, the stress in the diaphragm will go to
zero when the temperature decrease in the frame and diaphragm is, from
Equation 15:

$$-\Delta T_{max} = \frac{1.35 \times 10^{4} (1 - .3)}{10^{-6}(30)(10^{6})} = 314.5^{o}F \text{ decrease}$$
$$= 175^{o}C \text{ decrease}$$

The minimum operating temperature would be $-175^{o} + 20^{o} = -155^{o}C$.

If we permit the diaphragm stress to increase to 17,000 PSI, the maxi-
mum temperature rise above $20^{o}C$ would be for $\Delta S = +3.5 \times 10^{3}$ PSI.

$$+ T_{max} = \frac{3.5 \times 10^{3} (.7)}{30} = 81.5^{o}F \text{ rise}$$
$$= 45.3^{o}C \text{ rise}$$

The estimated steady state operating temperature limits for the bread-
board transducer with an iron diaphragm is:

$$T_{max} \cong 65^{o}C, \quad T_{min} = -155^{o}C$$

A change in the initial tension at room temperature can change the temper-
ature limits with a small effect on the temperature range.

A preliminary investigation of commonly available frame materials to
match a silver diaphragm indicate a much closer match of linear expansion
coefficients may be obtainable with stock materials. Aluminum and copper
base alloys are numerous which appear to have matching coefficients.[19] A
detailed investigation of published data is required for confirmation of
this impression. The lower Young's Modulus of silver is also favorable
for a wide operating temperature range. If we consider the operating
temperature range desired to be +250°C to -195°C, we can solve for the per-
missible maximum temperature coefficient differential between the frame
material and the silver diaphragm. The temperature limits were chosen by
the following operating conditions:

$250^{o}C$ = 10,000 hour life limit for the electrical insulation

$-195^{o}C$ = Boiling point of nitrogen at one atmosphere pressure

$$\Delta\alpha_{max} = \frac{\Delta S_{max} \ (1-\nu)}{\Delta T_{max} \ E} \qquad\qquad Eq \ (16)$$

For silver

$E = 11 \times 10^6$ PSI

$\alpha = 10.9 \times 10^6 /^{\circ}F$

$\nu \sim .3$

$S_{max} = 12,000$ PSI

$\Delta T_{max} = 250 + 195 = 445^{\circ}C = 800^{\circ}F$

$\Delta\alpha_{max} = \dfrac{1.2 \times 10^4 \ (.7)}{8 \times 10^2 \times 1.1 \times 10^7} = .955 \times 10^{-6}/^{\circ}F$

$\qquad\qquad \cong 1 \times 10^{-6}/^{\circ}F$

It is apparent that silver is more permissive of a temperature coefficient mismatch with the frame material. It does seem possible to obtain suitable available frame material with a temperature coefficient difference of $10^{-6}/^{\circ}F$.[19]

It is recommended a silver diaphragm be substituted in the present breadboard frame material for preliminary evaluation even though a large temperature coefficient difference does exist with AISI-310 alloy.

Prestressing the diaphragm maintains each element of the diaphragm in a plane when pressures are balanced by the closed loop servo system since compressive buckling stresses do not exist in the diaphragm.

Changes in diaphragm tension and stiffness caused by temperature do not effect the ability to correctly resolve ΔP since the diaphragm pressure is determined by a direct, identical electromagnetic substitution of ΔP.

The gas temperature and radiant temperature exposure of a nude pressure balancing ΔP sensor may vary drastically on initiation of a rocket engine test firing. In cases where the absolute pressure is high (10^{-5} torr or greater) and ablative particles are numerous, good operation may not be possible. The ΔP sensor should be properly shielded with high vacuum conductance massive heat shields for severe operating exposures. The large magnets used on the breadboard model as shown in Figures 2, 3 and 4 and the added perforated electric shielding plates over the outside capacity position sensing electrodes will serve as a very effective double radiant shield for the diaphragm. In addition, the massive performated diaphragm position sensor electrodes act as a third radiant shield to protect the diaphragm from external radiant heat sources. It is expected that the triple shielding will establish pressure measurements referred to the frame temperature of the pressure transducer. An imbedded thermistor temperature sensor can be used to measure the frame temperature for calculation of pressure-temperature transformations. The vacuum pressure time constant of the heat shields and instrument chamber volume should satisfy the speed of response requirement of the desired ΔP measurement. Cryo-

genic heat shields and instrument mounting are especially effective in suppressing thermal transient disturbances because of the high thermal accommodation coefficient for hot molecules striking the cryogenic surface. Cryogenic shields are, therefore, attractive to use on ΔP instruments measuring pressures at or near cryogenic surfaces in the test chamber. It is possible to determine the pressure of known gas species at other temperatures in molecular flow by calculation from the cryogenic pressure measurement.[20] In practice, this may be complicated where unknown mixed species exist and the low accommodation coefficient of some gases such as hydrogen and helium exist as important constituents.

3.1.8 Pressure Measurement at High Temperature

Pressure at known higher temperatures can be measured with a minimum effect of thermal transients by providing a massive high vacuum conductance heat shield and a transducer mount maintained at the desired temperature by a precision temperature controller. The desired temperature for measurement is determined by a temperature measurement at a corresponding location during a test firing and the transducer temperature controller is set to this temperature. Sufficient warmup time must be allowed to assure stabilization of controller temperature. Pressures may be measured by this method for temperatures up to the operating limits defined by materials used in transducer construction, approximately 200 to 300°C. Pressure at higher temperature may be calculated from this pressure measurement based on assumed or known gas composition.

The pressure temperature exposure limits for a nude pressure balancing gauge may be determined from the time constant of the transducer diaphragm immersed in a gas of known conductivity. The time constant, $1/\beta$ for typical gases in molecular conductivity with an illustrative transducer diaphragm are given in Appendix B. The temperature change, ΔT_d, of the transducer diaphragm during a test interval for a sudden step in gas temperature ΔT_d is:

$$\Delta T_d = \Delta T_g (1 - e^{-\beta\tau}) \qquad\qquad \text{Eq (17)}$$

ΔT_d must be less than the design ΔT_d max of the prestressed diaphragm for accurate pressure measurements.

A detailed study and numerical solution for ΔT_d effects due to current heating and environmental exposure are given in Appendix A.

3.1.9 Diaphragm Deflection

The maximum on axis deflection, Z, for a clamped circular diaphragm is[9]:

$$\frac{Wa^4}{Et^4} = \frac{16}{3(1-\nu^2)} \left[\left(\frac{Z}{t}\right) + .488 \left(\frac{Z}{t}\right)^3 \right] \qquad\qquad \text{Eq (18)}$$

Reference 9, pg. 220.

where: W = unit load, psid

a = radius of diaphragm, inches

E = modulus of elasticity, psi

t = thickness of diaphragm, inches

ν = Poisson's ratio

Z = maximum deflection, inches

For the breadboard model:

The deflection of a 2.645 inch diameter pure iron diaphragm .0005 inch thick with 1 mm Hg ΔP (1.93×10^{-2} psid) pressure is obtained with Equation 18.

$$\frac{1.93 \times 10^{-2}}{30 \times 10^6 \times (5 \times 10^{-4})^4} = \frac{16}{3(1-.09)} \left[\left(\frac{Z_{max}}{t}\right) + .488 \left(\frac{Z_{max}}{t}\right)^3\right]$$

$$\frac{Z_{max}}{t} \cong \sqrt[3]{3.6 \times 10^3} \cong 15.32$$

$$Z_{max} \cong 7.66 \times 10^{-3} \text{ inches deflection for 1 mm Hg } \Delta P$$

This unrestrained deflection would exist for 1 mm Hg ΔP unless opposed by an equal electromagnetic pressure.

3.2 DIAPHRAGM STRESS

A Teflon[(R)] or Paralene[(R)] coated backing plate will prevent frictional clamping and will limit the diaphragm maximum stress to S_{max} for a maximum deflection, Z_{max}; a design Z_{max} of 5×10^{-3} inches was used on the breadboard model stop plate:

$$S_{max} = \frac{Et^2}{a^2} \left[\frac{Z_{max}}{t} + \frac{1}{2}\left(\frac{Z_{max}}{t}\right)\right]^2$$

for Z_{max} = .005 in.

$$S_{max} = \frac{30 \times 10^6 (5 \times 10^{-4})^2}{(1.32)^2} \left[10 + 50\right] = 240 \text{ psi}$$

The factor of safety is:

$$\frac{42000}{S_{max}} = \frac{42000}{240} = 175 \text{ times}$$

The stop plate clearance in this case was selected to obtain high deflection sensitivity of the capacitance position sensor. The insulated

diaphragm stop plate is also the capacitance position sensor plate. When the diaphragm motion is restrained by the stop plate it does not short electrically to the plate because a high temperature low vapor pressure insulating film is applied to the stop plate and diaphragm surface. The diaphragm stop plate is perforated with .040" dia. holes spaced .070" between centers to obtain good vacuum flow conductance and consequently fast pressure transient response. The .040" dia. hole was selected experimentally to permit 60 psi overpressure applied to the diaphragm without visible marking or damage to the diaphragm.

3.2.1 Electric Field Transducer

The electric field pressure on a solid conducting charged surface is[1]

$$\overline{P}_e = \frac{\epsilon \overline{E}^2}{2} \qquad (19)$$

for vacuum or low pressure gases $\epsilon \approx 8.85 \times 10^{-12}$ farads/meter.

The electric field, $\overline{E}_{za}$, required for one atmosphere electric pressure (P_{za}) on a conducting boundary in the X-Y plane is from Equation 19:

$$P_{za} \approx 1.02 \times 10^5 \text{ newtons/m}^2 \text{ at one atmosphere}$$

$$\overline{E}_{za} = \sqrt{\frac{2 \overline{P}_{za}}{\epsilon}}$$

$$\overline{E}_{za} = \sqrt{\frac{2 (1.02) (10^5)}{8.85 \times 10^{-12}}} = 1.52 \times 10^8 \text{ volts/meter at one atmosphere}$$

The disruptive field strength is proportional to the absolute pressure for pressures exceeding a few mm of Hg and is approximately 3×10^6 volts/meter for air at one atmosphere. However, practical considerations require the maximum electric field to be less than 3×10^6 volts/meter. At lower vacuum pressures the disruptive electric field strength becomes very high. Hence, an electric field pressure is not suitable for restoring pressure at absolute differential pressures above a fraction of an mm of mercury because the required electric restoring force field exceeds the disruptive field unless the reference pressure is a very high vacuum. The current sheet pressure balancing transducer is not disabled at high pressures except by Joule heating due to current flow which may cause excessive diaphragm temperature rise at higher differential pressures.

3.2.2 Sensor Pressure Sensitivity

The sensitivity of an ac capacitance bridge position error sensor is proportional to the capacitance electrode area and the maximum electric field intensity permissible without conductive leakage and/or ionization to the capacitance electrode. The disruptive uniform electric field intensity for one atmosphere is approximately 3×10^6 volts per meter. The disruptive electric field strength is proportional to pressure provided

the electrode spacing is many times the mean free path of the gas molecules. Close capacitance electrode spacing will enable the critical disruptive electric field to be much higher than 3×10^6 volts per meter for moderate and low absolute pressure. If the electrode spacing is sufficiently close, a large margin of safety on capacitance electrode leakage can be realized at 1 mm of mercury absolute pressure. For example, consider a working capacitance electric field intensity:

$$E \sim \frac{3 \times 10^6}{760} \sim 3 \times 10^3 \text{ volts/meter}$$

A constant current capacitance electrode supply will maintain a constant electric field intensity for all diaphragm positions and will provide a bridge unbalance voltage proportional to electrode clearance. Consider the following conditions:

Computed diaphragm deflection for 1 mm Hg ΔP,

$Z_{max} = 5.8 \times 10^{-3}$ inches $= 1.473 \times 10^{-4}$ meters.

Diameter of capacitance sensor electrode =

1.75 inches $= 4.45 \times 10^{-2}$ meters.

The open circuit output voltage change, ΔV_o, due to an average diaphragm area deflection equal to 1/3 the maximum deflection for 1 mm Hg ΔP is:

$$\Delta V_o = E_z Z \sim 3 \times 10^3 \left(\frac{Z_{max}}{3}\right) \sim Z_{max} \times 10^3 \text{ volts}$$

$$\Delta V_o = 1.473 \times 10^{-4} \times 10^3 = .1473 \text{ volts/mm Hg } \Delta P.$$

where 3×10^3 volts/meter is the selected capacitance electrode electric field intensity.

Commercial synchronous detection ac voltmeters are available which will measure 10^{-9} volt signals with good accuracy when the correlation interval is at least 1 second. It is reasonable to expect a specialized design synchronous ac amplifier may perform better. For the available 10^{-9} volt sensitivity, the pressure sensitivity would be:

$$\Delta P \text{ min.} = \frac{V_{o \text{ min.}}}{V_{o \text{ 1 mm Hg}}}$$

$$\Delta P \text{ min.} = \frac{10^{-9}}{.1473} = 6.78 \times 10^{-9} \text{ mm Hg } \Delta P$$

The dielectric strength of the capacitor sensor in high vacuum will be much greater than is realized at lower pressure, hence it is easily possible to expand the sensor sensitivity 1000 times for high vacuum by increasing the sensing capacitance supply current 1000 times. The operating field intensity is increased from 3×10^3 volts/meter to 3×10^6

volts/meter for pressure ranges from 10^{-9} mm of Hg to 10^{-12} mm of Hg. The expanded sensitivity should only be used for a capacitor sensor supply when the absolute pressure $\leq 10^{-8}$ mm of Hg.

The performance estimates indicate measurement of a differential pressure range of 1 mm Hg to 10^{-12} mm is possible. The high pressure range which may be much greater than 1 mm of Hg is limited by diaphragm buckling due to thermal expansion caused by restoring current Joule heating. The high pressure limits and errors require further design study and experimental evaluation. The low differential pressure limit will be determined by external disturbances, electronic circuit noise and fluctuations due to the statistical variation of internal and external molecular impacts on the sensor diaphragm.[10]

3.2.3 Experimental Pressure Sensitivity

The amount of effort available for experimental evaluation and development of the pressure balancing transducer pressure sensitivity was limited by the amount of effort required for the transducer design and construction and evaluation of the breadboard current deflection sensitivity.

Bridge circuits were tried within the pressure sensor which used the PAR Type A differential amplifier directly as a bridge unbalance detector in the differential mode with a transformer bridge driver coupled to the PAR HR-8 reference generator output. This circuit was limited by the grounding requirement for the common differential input terminal of the Type A amplifier and a maximum common mode suppression of 40 Db. The ac common mode error of the Type A differential amplifier may be suppressed by a circuit similar to Figure 6 but the common input ground requirement for the Type A amplifier would prevent grounding the diaphragm current driver amplifier. A circuit similar to Figure 7 was tried using quality commercial audio transformers. These transformers did not perform well with respect to balance, common mode suppression and noise pickup. This experience led to the application of transformers specially designed for the ac carrier capacitance bridge circuit and to the circuit design shown in Figure 7.

The circuit in Figure 7 with the components specified appears to perform well and considerable experimental evaluation and adjustment is necessary before the performance potential is fully realized. Reducible odd harmonic 60Hz noise pickup still exists which can be reduced by improved grounding, layout and shielding. Acoustic noise and vibration coupled to the transducer from the environment and mounting must also be isolated.

The pressure transducer flange was mounted to the top plate of a double ended bell jar for initial low pressure ΔP tests. The conducted vibration from the pump and building limited the ΔP error balance that could be obtained on the capacitance diaphragm position error sensing circuit. This acoustic and vibration noise can be greatly reduced by

U.T.C.
DO-T-23

TO REFERENCE OSC
OUTPUT JACK
PAR MODEL HR-8

800/1200 CT
10K
2.7K
.02UF
1K

AT PAR HR-8
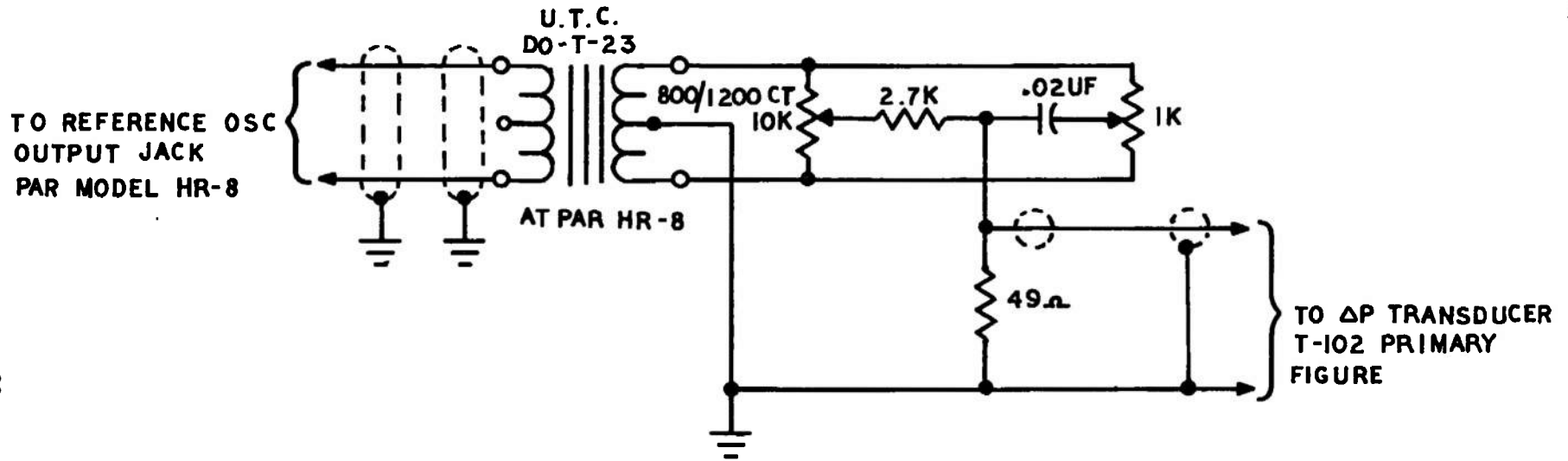
49 Ω

TO ΔP TRANSDUCER
T-102 PRIMARY
FIGURE

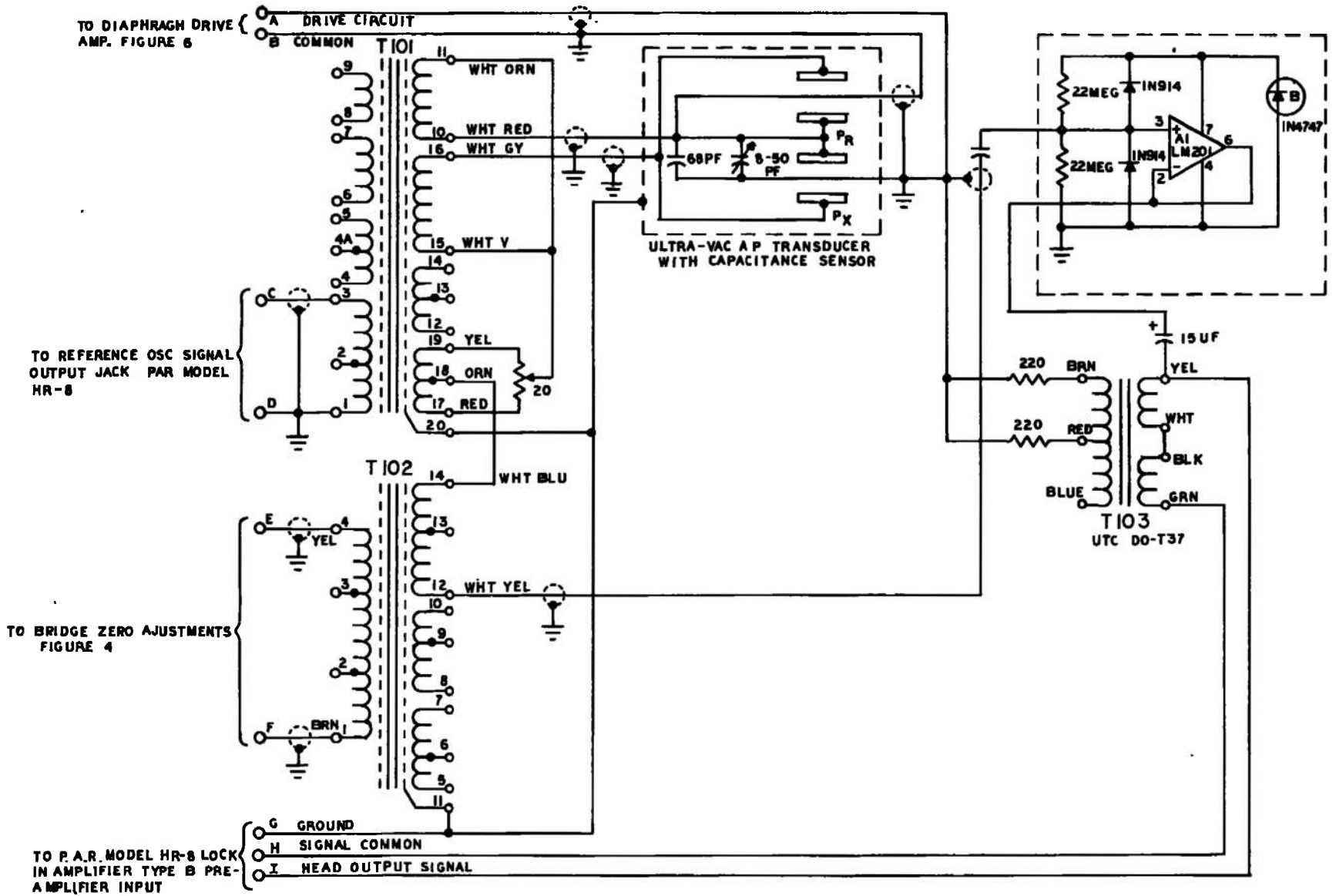FIGURE 6 ΔP TRANSDUCER NULL BALANCE CIRCUIT

Figure 7.   Pressure Head Schematic.

mounting the transducer in high vacuum on a vibration isolating damped wire suspension.

Sufficient sensitivity and signal level were obtained from the transducer position error sensor circuit of Figure 7 for all measurements which were completed by omitting the operational amplifier follower circuit shown and connecting the capacitance bridge circuit output directly to the PAR-HR-8 Type B amplifier input. The hybrid bridge transformer T-101 of Figure 7 was driven by 1 volt rms from the PAR HR-8 internal reference signal source. An output sensitivity directly into the Type B amplifier of 640 millivolts/volt/mm ΔP at low ΔP's was measured, referred to the primary voltage of T-101. The dynamic range measured at laboratory atmosphere environment was .0023 mm to 1 mm ΔP with no evidence of hard limiting for higher than 1 mm ΔP. The low pressure limit observed was established by ambient noise and acoustic vibration conditions for the setup used. A setup with adequate vibration, acoustic and electric isolation can be expected to utilize more fully the sensitivity limit of the PAR-HR-8 amplifier for very low ΔP's. It is apparent that the increased output filter time constant required to measure very low ΔP's will require development of bridge balancing techniques which are practical when very slow output response observations only are available. In the absence of external electrical and acoustic disturbances, the PAR-HR-8 amplifier and Type B preamplifier without the LM 201 follower amplifier preceding it would be capable of measuring a full scale ΔP of 1.56×10^{-9} mm of Hg. The LM 201 follower amplifier is expected to improve the actual attainable low limit ΔP as limited by ambient electrical and acoustic noise levels.

The conclusion resulting from the small amount of experimental evaluation of ΔP sensitivity limit is: (1) experimental work must be done to reduce the effect of ambient electrical, acoustic and vibration noise; (2) techniques must be developed for balancing the pressure sensor bridge circuit when slow response indicator systems are required to eliminate undesired noise disturbances; and (3) the changes in bridge balance between high vacuum zero ΔP conditions and high pressure zero ΔP conditions must be made negligible by a suitable mechanical adjustment and other compensation of the capacitor sensor plates on the transducer. This effect is believed due to a capacity unbalance between the inner sensor plates and the exterior sensor plates.

3.2.4 Response to Pressure Transients

It is desirable to have a high fidelity readout of rapid changes in pressures. The response to rapid changes corresponds to the requirements met by a high quality diaphragm type condenser microphone used as a standard for acoustic pressure measurements[13]. Acoustic standard condenser microphones are capable of making uncorrected calibrated acoustic pressure measurements for frequencies of a few hertz to 20 kilohertz.

Condenser microphones include acoustic elements dependent upon normal atmospheric pressure and composition to achieve this excellent performance, however, excellent results can also be obtained using diaphragm

gauges for low vacuum pressure measurements. In addition, the gauges are
able to accurately measure static or dc differential pressure. Because
of variable and low absolute pressure encountered, acoustic correction
elements cannot be used to obtain high fidelity readout of fast or slow
changing ΔP functions. Negative feedback of the pressure error function
can improve stability, speed of response, and precision in low pressure
diaphragm gauges. The negative feedback will also damp the high Q natural
diaphragm resonances when high gain, high stability servo systems are
used.

The force applied to a point in a linear mechanical system is given
by DeAlamberts' equation for one dimensional motion:

$$F = kx + b \ \frac{dx}{dt} + m \ \frac{dx^2}{dt^2} + C \ (t)$$

where:

F   = force

k   = spring stiffness or constant

x   = particle deflection from reference position

b   = viscous damping or mechanical resistance

t   = time

m   = mass at the point

C(t)= constant or variable force function applied at the point

The force given for one dimensional motion must be integrated through-
out the volume of a linear elastic solid in three dimensions to obtain the
equation of motion and deflection of any point in a three dimensional
body. This problem has been solved for an elastic disc clamped at the
edge in vacuum[11],[12].

For the diaphragm dimensions selected for illustrative performance
calculations on Page 13 of this report, the radial resonant frequencies
in vacuum are[11] for an iron diaphragm in CGS units. The first radial
mode resonant frequency is:

$$f_o = 2.50 \times 10^5 \ t/a^2 \qquad (20)$$

The second radial mode resonant frequency is:

$$f_1 = 5.27 \times 10^5 \ t/a^2 \qquad (21)$$

The third radial mode resonant frequency is:

$$f_2 = 9.63 \times 10^5 \ t/a^2 \qquad (22)$$

For the diaphragm dimensions selected for the breadboard model, we obtain:

$$t = 5 \times 10^{-4} \text{inches} = 1.27 \times 10^{-5} \text{cm}$$

$$a = \frac{2.645}{2} \text{ inches} = 3.36 \text{ cm}$$

from Equation 19:

$$f_o = \frac{2.5 \times 10^5 (12.7 \times 10^{-4})}{(3.36)^2} = 31 \text{ Hz}$$

This resonant frequency is computed for the breadboard diaphragm without tension; a small tension which must exist for satisfactory sensor operation will increase the resonant frequency.

At a frame and ambient temperature where the breadboard model iron diaphragm stress is 11,000 psi, the following resonant frequency is obtained:

For:

$s = 11,000$ psi; $a = 3.36$ cm; $t = 1.27 \times 10^{-3}$ cm

$\rho = 7.86$ gm/cm^3, $\sigma = \rho t = 1.27 \times 10^{-3} \times 7.86 = 9.98 \times 10^{-3}$ gms/cm^2.

s dynes/cm$^2 = \dfrac{11,000}{2.248 \times 10^{-6}(2.54)^2} = 7.6 \times 10^8$ dynes/cm^2

$T = st = 7.6 \times 10^8 \times 1.27 \times 10^{-3} = 9.66 \times 10^5$ dynes/cm

The fundamental resonant frequency of a taut diaphragm is[12]:

$$f_o = \frac{.38274}{a} \sqrt{\frac{T}{\sigma}} \tag{23}$$

For the conditions selected on the breadboard iron diaphragm:

$$f_o = \frac{.383}{3.36} \sqrt{\frac{9.66 \times 10^5}{9.98 \times 10^{-3}}} = 1.123 \times 10^3 \text{Hz}$$

The substitution of a silver diaphragm is recommended to improve performance of the breadboard model. For a taut silver diaphragm substitution in which:

$a = 3.36$ cm; $t = 1.27 \times 10^{-3}$cm; $\rho = 10.5$ gms/cm^3

$E = 11 \times 10^6$ psi; $S_{max} = 25,000$ psi; $S_{yield} = 12,000$ psi

$S_{operating} \overset{\sim}{=} 10^4$ psi

$\sigma = \rho t = 10.5 \times 1.27 \times 10^{-3} = 1.33 \times 10^{-2}$ gms/cm^2

$S_{max} = t.92 \times 10^8$ dynes/cm^2

$$T = St = 6.92 \times 10^8 \times 1.27 \times 10^{-3} = 8.78 \times 10^5 \text{ dynes/cm}$$

Hence for a silver diaphragm:

$$f_o = \frac{.383}{3.36} \sqrt{\frac{8.78 \times 10^5}{1.333 \times 10^{-2}}} = 922 \text{ Hz}$$

The resonant frequency of the taut silver diaphragm is approximately 10 percent less than the iron diaphragm. This is satisfactory.

A typical unloaded in vacuum frequency response of the diaphragm with low tension is shown in Figure 13. The frequency response is flat to dc or static pressures. The actual unloaded response to higher order radial and circumferential modes is dependent upon the size and shape of the position sensing electrode. It is possible to nullify a higher order mode response peak by proper selection of the position sensor electrode geometry.

When a conducting magnetic diaphragm in a strong magnetic field is externally short circuited by the electric driving source impedance, the resonant peaks are highly damped by the induced current flow caused by the diaphragm velocity in a magnetic field. The effect of the magnetic damping on the free response of Figure 8 is shown in Figure 9. The flat frequency response can be extended to the second radial resonance by closed loop operation with a properly designed servo system as shown in Figure 9. The extended bandwidth operating mode may be usable where sufficient ΔP exists to override noise disturbances. Essentially, ballistic or integrating low speed response which is flat for slow speed and static differential pressures is required to resolve very low differential pressures approaching 10^{-12} mm of Hg. Higher ΔP's can therefore be resolved with an increased bandwidth or speed. Figure 10 shows a typical time function response to a unit step pressure input function for the pressure balancing transducer in the damped and extended bandwidth mode. The undamped pressure step response is not shown because the "ringing" of the diaphragm would be of large amplitude for a long time period when damping is excluded. The response functions shown in Figure 14 are for the pressure excitation function applied directly to the diaphragm. The time constant of the sensor chamber volume and the vacuum conductance of the sensor pressure ducts and heat shields may affect the indicated system response unless they are properly constructed.

The response characteristics shown in Figures 8, 9 and 10 are for a clamped disc with low tension. Prestressing is useful for eliminating the effects of temperature changes and will be used in the transducer diaphragm. The initial tension will improve the response speed and extend the frequency response with a sacrifice in sensitivity. The absolute ΔP calibration is not affected by diaphragm tension since the ΔP measurement is made by a direct and identical substitution of an opposing electromagnetic pressure.
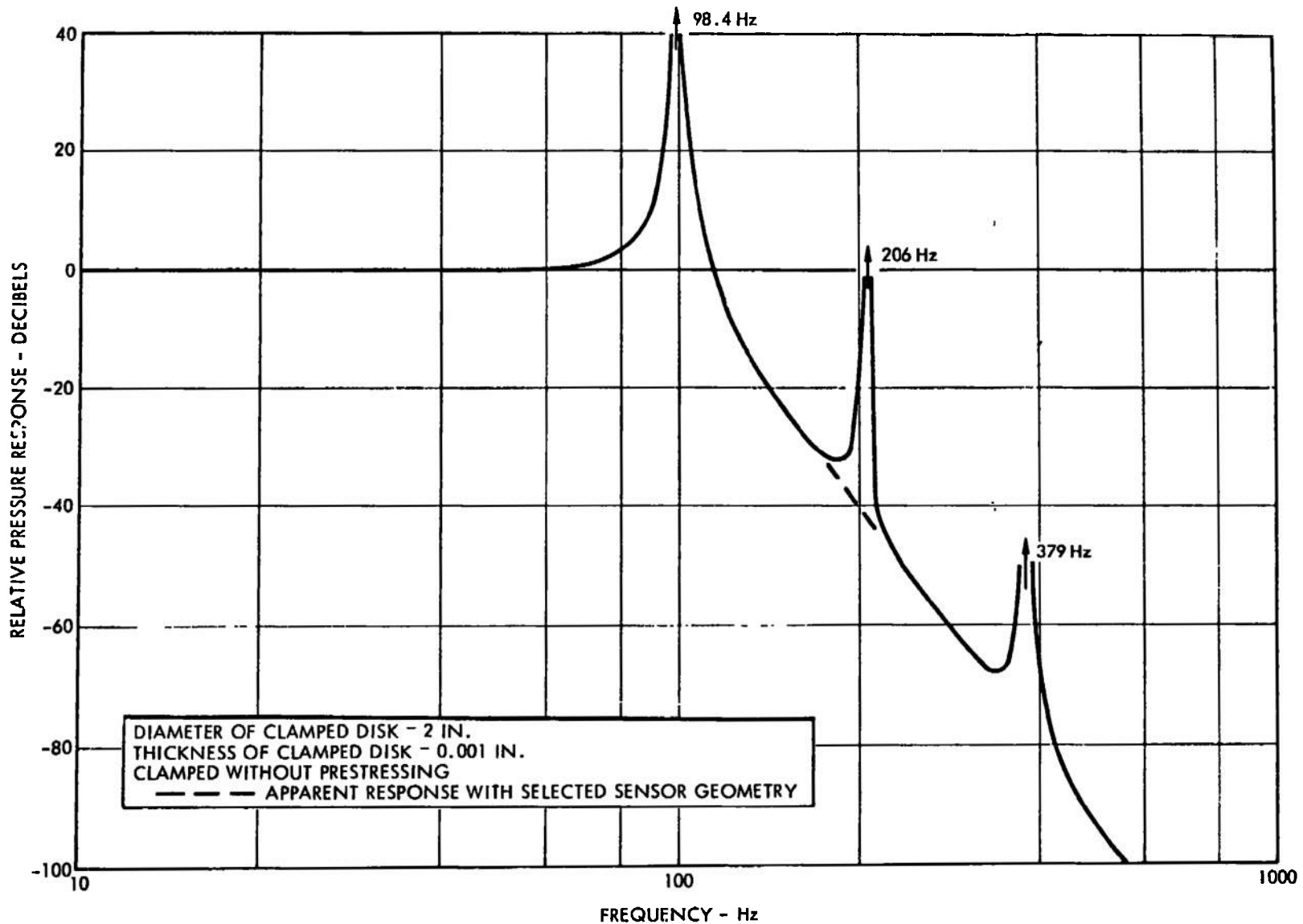
Figure 8. Open Loop, Unloaded, Undamped Pressure Frequency
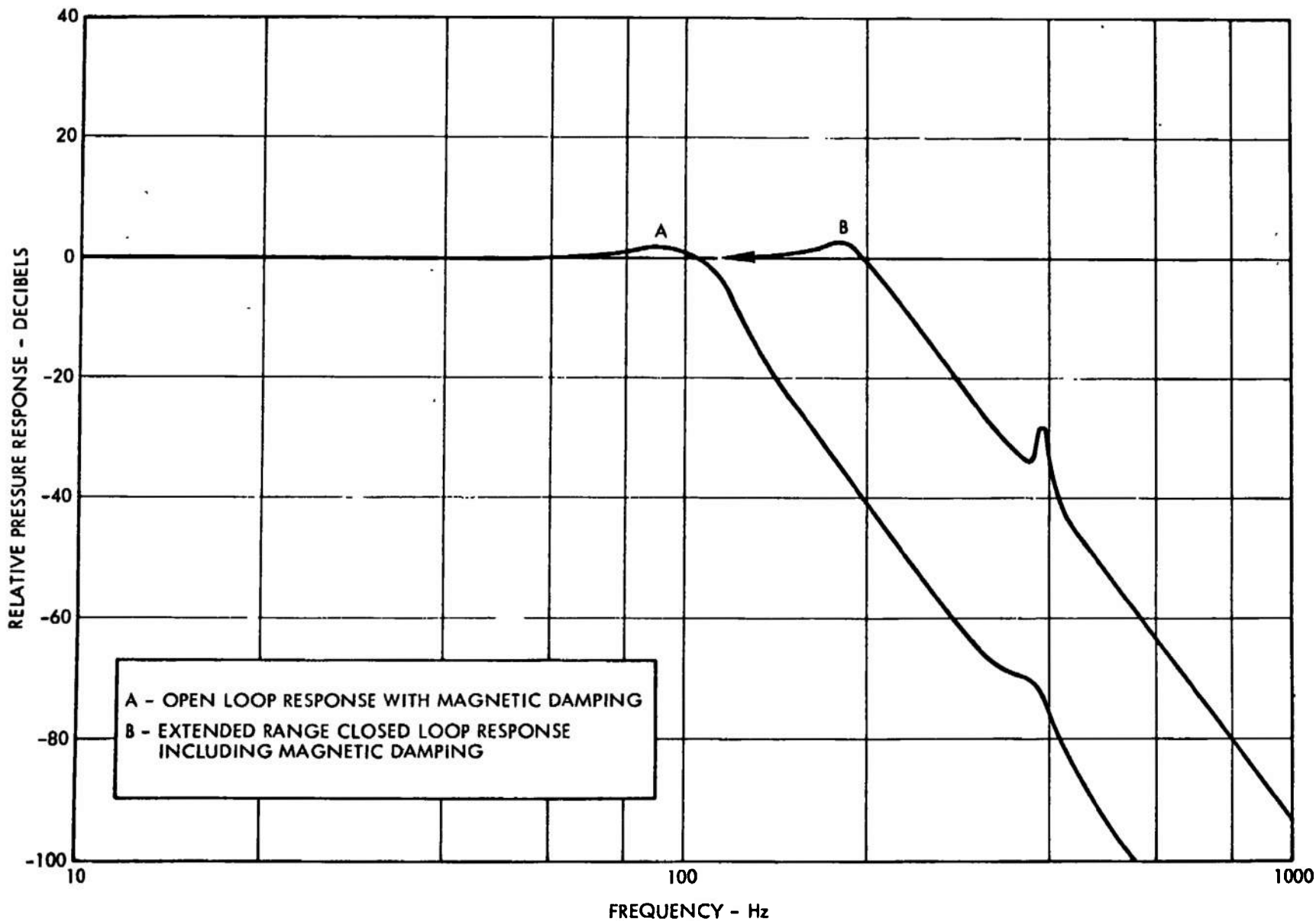Response of a Typical Iron Diaphragm in Vacuum

Figure 9. Typical Pressure Frequency Response
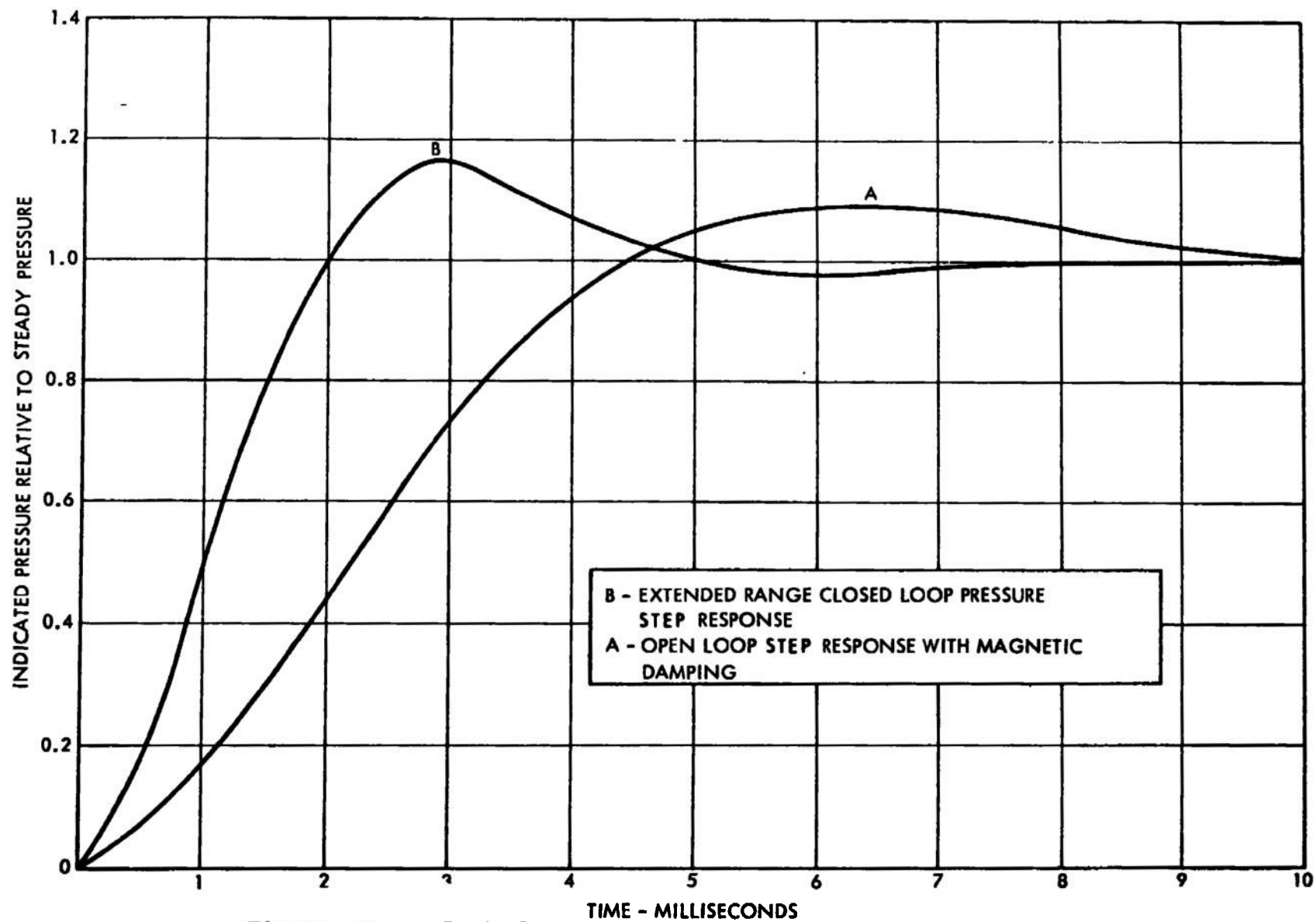for a Pressure Balancing Transducer

AEDC-TR-71-144

Figure 10.   Typical Response of a Pressure Balancing
Transducer to a Step Pressure Change

3.2.5 Electronic Test and Control Circuits

A closed-loop electronic control system similar to Figure 5 is suitable for the self-balancing pressure meter. The initial test and evaluation objectives can be met by adapting commercially available electronic equipment for this application. The electronic amplifier and indicator (MKS Type 77M)[5] supplied with the MKS Type 77H diaphragm pressure transducers were considered for the initial tests because the essential circuit functions, including the oscillator, carrier amplifier, synchronous detector and output filter, were included. The initial tests made with the MKS Type 77M indicator unit have shown the open-loop gain and signal-to-noise ratio were not suitable for the desired closed-loop system dynamic range and resolution requirement.

Subsequent to evaluation of the MKS Type 77M indicator unit, a PAR Model HR-8 precision synchronous amplifier was acquired for use on this project. This amplifier is very suitable for the pressure balancing transducer experimental evaluation because of the great flexibility in adjustment of operating parameters. The features include:

1) Carrier frequency continuously tunable from 1.5 Hz to 150 KHz.

2) Noise rejection at synchronous frequency 59 Db below ambient noise in a 1 KHz bandwidth.

3) Output Filter – Choice of single or cascade low pass networks with adjustable time constants from 1 millisecond to 100 seconds.

4) Output Stability – .1 percent of full scale.

5) Gain Stability – $\pm.4$ percent at 400 Hz (Q of ten).

6) Linearity – $\pm.1$ percent of full scale.

7) A choice of input preamplifiers and sensitivities are available to obtain high sensitivity and a good noise figure.

The following preamplifiers were selected:

Type A preamplifier with adjustable full-scale sensitivities of 100 nanovolts to 500 mv.

Type B (low impedance) with adjustable full-scale sensitivity of 1 nanovolt rms to 5 millivolt rms with 100/1 transformation ratio.

8) Selectivity – Equivalent adjustable Q of 5 to 25 for the carrier amplifier.

9) Zero Suppression – Adjustable calibrated DC output offset from zero to 1000 percent of full scale.

10) Outputs

   a) A 1/2 percent linear panel meter with choice of center or left-hand zero.

   b) Front panel output monitor jack ± 10 volts full scale.

   c) Rear terminal outputs – Adjustable recorder output ± 10 volts full scale.

11) Monitor – A switch allows connection of the output meter to the signal amplifier output, reference signal output, mixer output and integrator amplifier output.

12) Internal Calibrator – A built-in standard source for gain and sensitivity calibration from 20 nV to 100 mV rms fundamental frequency component.

13) Reference Signal Channel – This channel provides for four operating modes—external reference, internal reference, automatic external reference control and a selective external reference frequency.

14) Phase Shifter – The phase shifter permits 0 to 360° adjustment of the reference signal phase to enable maximum synchronous detector output.

The PAR Model HR-8 Amplifier has been found very suitable for all open and closed-loop tests performed on this program with the following exceptions: The 360-cycle power line noise from the amplifier and internal reference channel can cause noise overload in some very high gain closed-loop measurements. This noise is probably due to harmonic electromagnetic coupling from the built-in 60 Hz power supply transformer. The single and cascade output amplifier filters pass a large amount of the synchronous demodulator output switching spikes. These amplifiers do not reject the high frequencies in the manner of an ideal integrator and hence would cause carrier feedback and oscillation if the transducer or transducer simulator utilized the built-in output filter due to carrier or reference frequency feedthrough during the closed-loop or pressure balancing mode of operation. Measurements on the signal channel selectivity have shown the selectivity curve attenuation and phase shift does not closely correspond to the selectivity and phase computed for an ideal constant Q selective circuit. This is not a serious matter because the Q adjustment and reference frequency adjustment can be experimentally changed to obtain stable closed-loop operation in the pressure balancing control system.

The 360 Hz internal noise overload was avoided during closed-loop tests by keeping the loop gain below the 360 Hz overload point. Higher loop gain may require a "bucking" 360 Hz signal if the 360 Hz noise is stable or operation from an external very high quality ± 24 volt power supply or battery supply will be required. A solution to the 360 Hz noise reduction may be determined during a continuation of this project.

The output amplifiers and filters in the PAR HR-8 amplifier serve
the intended open-loop operation functions very well. The closed-loop
operation of the pressure balancing transducer or simulator with the HR-8
required the construction of a separate single-stage, nearly ideal output
amplifier and integrator illustrated in Figure 11. A cascade 12 Db/octave
filter cannot be used for closed-loop operation because it will not
satisfy the Nyquist or Bode stability criteria[7,8] when operated on the
output of the HR-8 amplifier.

The input to the custom-built integrator amplifier is connected to
the recorder output terminals on the back of the HR-8. The internal
series loss resistor to the HR-8 recorder output terminals is bypassed
with a .076 uf capacitor to form the series branch of a 50 Db boost
phase lead network. The recorder output is terminated with 25 ohms to
complete the lead network. This network is necessary to compensate for
excess phase shift in the PAR-HR-8 at frequencies above 300 Hz and thus
enables stable closed-loop operation with high loop gain. The PAR-HR-8
internal time constant filters are switched to off when the amplifier
is operated in a closed-loop control system.

A diode ring balanced modulator was constructed to simulate the
pressure balancing transducer function prior to completion of transducer.
This circuit is shown in Figure 12. This modulator enabled simulated open
and closed-loop experimental studies with the pressure balancing control
system shown in Figures 13 and 14. The noise overload due to 360 Hz noise
pickup was observed with this system with high closed-loop gains. The
very low frequency loop gain at 360 Hz noise overload point was observed
to be 115 Db. The compensated stability limit loop gain was calculated
to be 237 Db. Subsequent experience has shown the noise overload point
can be greatly reduced by careful shielding and grounding and substitution
of higher quality transformers in the bridge and transducer circuits.
The pressure head circuit of Figure 7 illustrates the substitution of
improved transformers with a resulting large improvement in null balance
and noise pickup for the bridge circuit. Time did not permit detailed
evaluation of the transducer with improved circuit components. This
work must be done as part of a continuation effort. The outer capacity
pickup electrodes on the pressure transducer shown in Figures 2 and 3
do not have full electrical shielding. Temporary perforated metal
plate shields were fastened on the flange of the diaphragm tension rings
to fully shield these electrodes. These shields greatly reduce noise
pickup and also will act as an important radiant heat shield in addition
to the massive radiant heat and electrical shielding provided by the large
bias magnets.

3.2.6 Recommended Transducer Improvements

This report has considered details on the experimental performance
analyses which were done on the breadboard transducer. The significant
deviation from the proposed conceptual design performance is due to the
current deflection sensitivity which measured 30 times less than the
conceptual design performance calculation. The experimental investigation
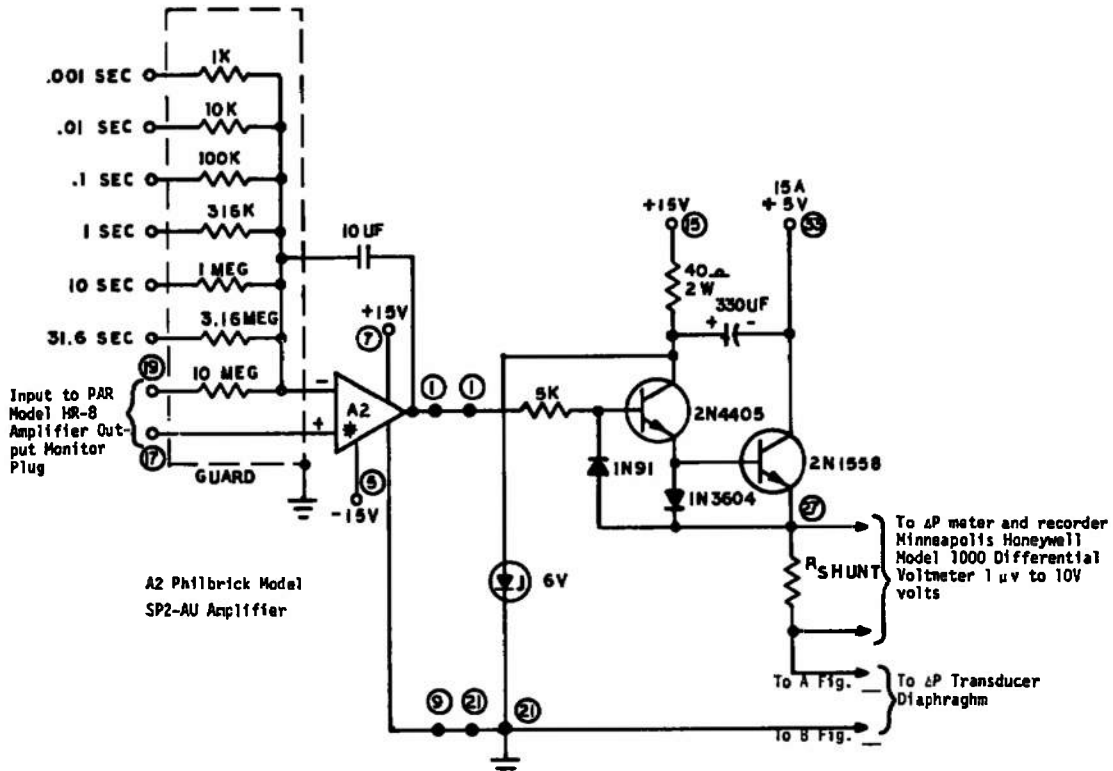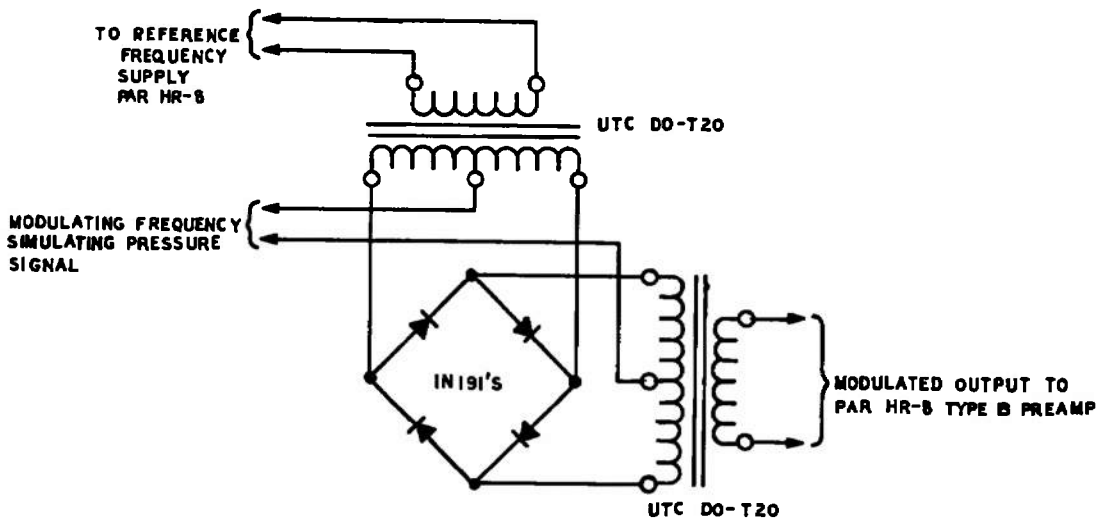
Figure 11. Output Filter and Driver Amplifier.

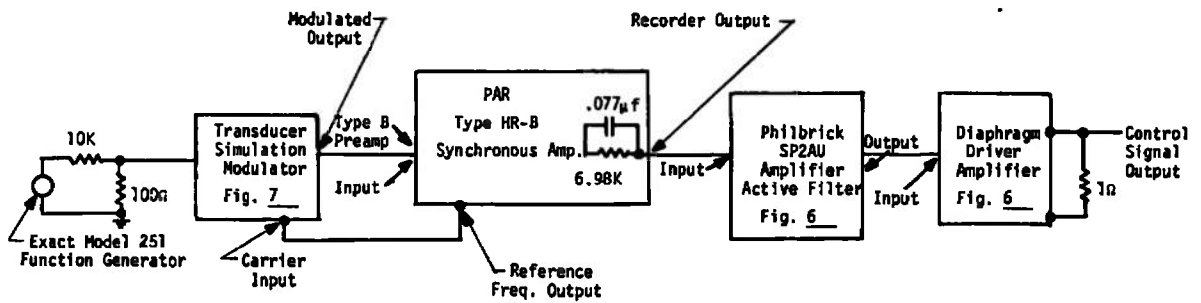Figure 12. Transducer Simulation Balanced Modulator.

Figure 13. Open Loop Pressure Balancing Control System Simulation.
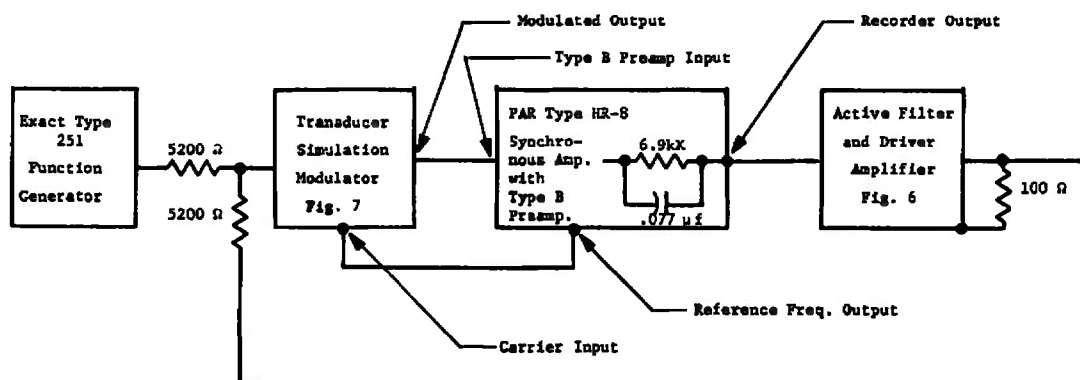

Figure 14. Closed Loop Pressure Balancing Control System Simulation.

demonstrated the magnetic flux density tangential to the diaphragm should be used for electromagnetic pressure calculations instead of the magnetic flux density within the diaphragm. Consequently, the use of a magnetic diaphragm in the breadboard model did not produce the predicted enhancement in performance due to its high magnetic permeability and saturation flux density. Recognition of this factor has enabled the choice of silver as a new diaphragm material to obtain performance improvements due to several factors. The substitution of the silver diaphragm in the existing transducer frame will permit their experimental demonstration. A modification of the breadboard transducer frame to increase the tangential magnetic flux density will permit experimental demonstration of the third improvement possible with the silver diaphragm substitution. A fourth simple improvement which was demonstrated is the addition of perforated metal electric and heat radiation shields which are fastened to the flanges of the diaphragm tension control rings.

a) Increased Restoring Pressure Due to Current Density

The substitution of silver for the pure iron diaphragm reduces the heat generated by the pressure balancing current flow in direct proportion of the electrical resistivity of the diaphragm material.

Where:

ρ_{fe} = resistivity of pure iron = 10^{-5}ohm cm

ρ_{ag} = resistivity of pure silver = 1.47×10^{-6}ohm cm

The current density, J, can be increased with the silver diaphragm for the same heat loss

$$J_{fe}^2 \, \rho_{fe} = J_{ag}^2 \, \rho_{ag} \qquad\qquad (24)$$

$$\frac{J_{ag}}{J_{fe}} = \sqrt{\frac{10}{1.47}} = 2.61 \text{ times}$$

The restoring magnetic pressure for a given diaphragm current heating is increased 2.61 times by substituting a silver diaphragm for the pure iron diaphragm.

b) Reduction of Driving Current

The driving current required for a given restoring pressure can be reduced by reducing the width of the diaphragm transverse to the direction of current flow. A diaphragm width equal to the breadboard transducer clamp ring's outside diameter is recommended. The current is reduced by the ratio of the present iron diaphragm width to the recommended silver diaphragm width.

Iron diaphragm width = 4.25" = W_{fe}

Diaphragm clamp ring O.D. = 3.798" = W_{ag}

Driving current ratio for equal pressure

$$\frac{\dot{W}_{fe}}{W_{ag}} = \frac{4.25}{3.80} = 1.16 \text{ times}$$

The current is decreased 1.16 times by the recommended silver diaphragm width.

c) <u>Increase of Restoring Pressure by Flux Increase</u>

The breadboard diaphragm clamping frame can be modified by addition of magnetic inserts as shown in Figure 15 to increase the tangential flux density on the diaphragm. The tangential flux density ratio is approximately inversely proportional to the bias magnet gap ratio. The restoring pressure is directly proportional to the magnetic flux density.

Present breadboard magnet gap G_{fe} = 4"

Proposed modified breadboard magnet Gap G_{ag} = 2.75"

The tangential flux density ratio is:

$$\frac{B_{tag}}{B_{tfe}} = \frac{G_{fe}}{G_{ag}} = \frac{4}{2.75} = 1.453 \text{ times}$$

The change in magnet gap ratio will improve the restoring pressure 1.453 times.

After demonstration of the above improvements, it is recommended that a design study and detailed design be made with suitable frame material to minimize thermal stress changes over the desired operating temperature range,-195°C to 250°C, incorporating all of the above improvements. The wide temperature range design should be constructed when evaluation of the improved breadboard transducer and the associated electrical control system has been demonstrated to a desired degree.

The thermal stress in the improved transducer may be measured over the desired operating temperature range in a test chamber by measuring the resonant frequency of the diaphragm. The resonant frequency of the diaphragm is proportional to the square root of the diaphragm stress. The resonant frequency is readily measured by driving the diaphragm from a variable frequency constant current source and observing the lowest sensor frequency response peak. The completion of this work and the breadboard electronic control system improvement and evaluation should provide a reasonably complete and detailed foundation for the design and construction of the final prototype and test chamber hardware.
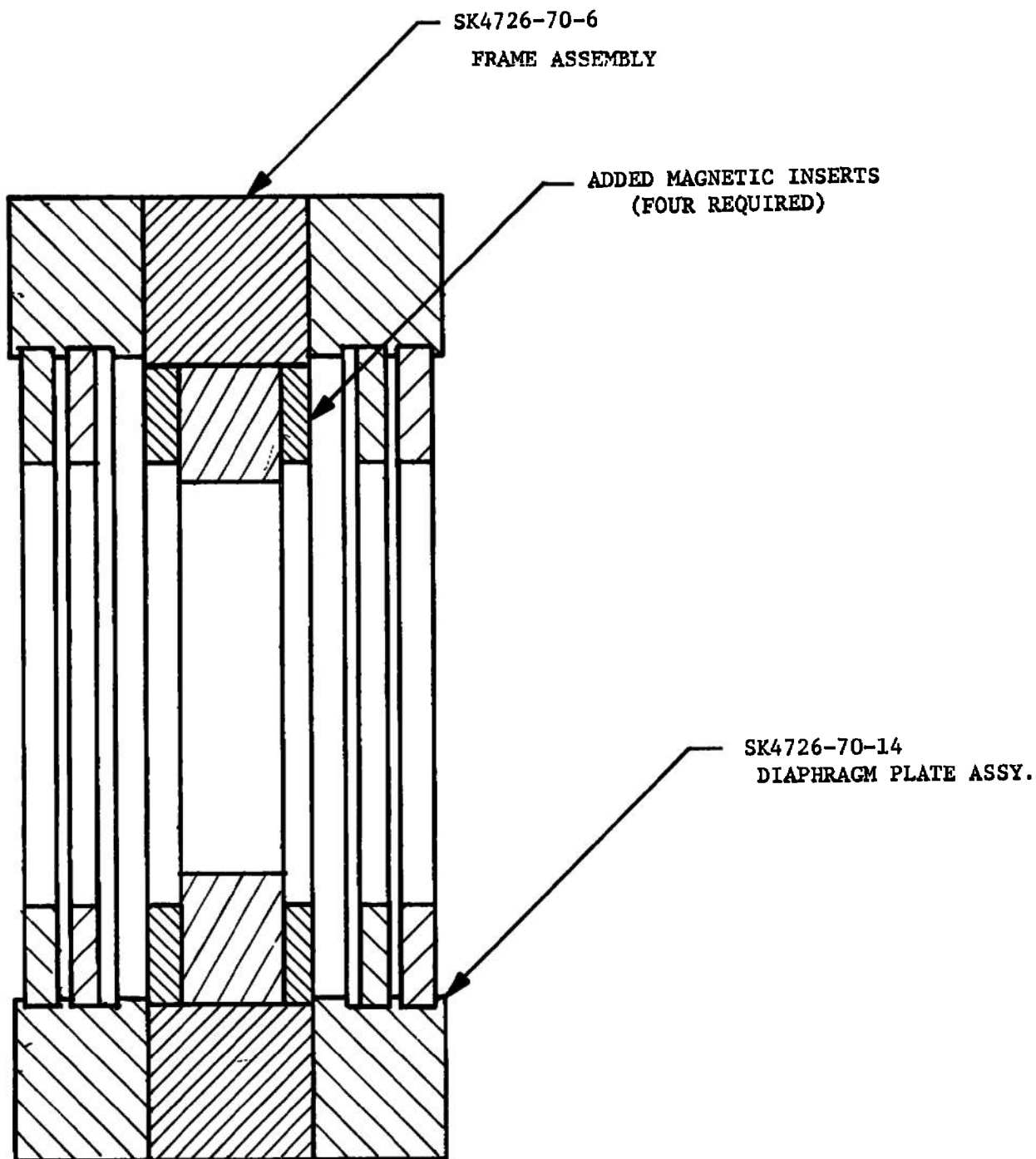
SK4726-70-6
FRAME ASSEMBLY

ADDED MAGNETIC INSERTS
(FOUR REQUIRED)

SK4726-70-14
DIAPHRAGM PLATE ASSY.

Figure 15. Cross Section of Improved Breadboard Transducer.

3.2.7 Transducer Fabrication Problems.

Most of the problems encountered during the breadboard transducer development were basic design and material selection problems. These problems were difficult and apparent in the design section of the report. The problems of fabrication were primarily problems of obtaining practical methods of fabrication for the desired performance requirements. Two requirements were most difficult to obtain: 1) high electrical insulation resistance between the diaphragm assembly and the clamping frame for all operating conditions with low vapor pressure and gas load due to the insulation; 2) immeasurable gas leakage between the closed interior reference pressure chamber and the exterior ambient pressure.

The application and processing of the low vapor pressure, high temperature polyimide varnish to the diaphragm and mating frame components was not an ideal smooth continuous film without conducting occlusions. This is due to limitations of the available manufacturing facility and insufficient development of detailed process procedures. A successful electrical insulation resistance after assembly was obtained after repeated trials.

The insulation resistance of the final diaphragm and frame assembly was measured with repeated exercising of the diaphragm by successive applications of 0 and 15 psid ΔP. The minimum insulation resistance measured was 1.3×10^{11} ohms with 40 volts test voltage.

The helium gas leakage was measured between the reference pressure chamber and the exterior by "bagging" the exterior with one atmosphere of helium and measuring the leakage to the reference pressure chamber on a helium mass spectrometer leakage meter. The leakage was below the minimum detectable level of 7×10^{-10} SACC He/second. This leakage level was the result of many assembly attempts to obtain acceptable gas leakage with the serated polyimide ring seals designed to seal the diaphragm area. After a design study, these seals were augmented by an additional Viton "O" ring seal and the low gas leakage level resulted.

The pressure and current deflection sensitivity have been discussed in detail in this report. The best measurements of these parameters were obtained by open loop measurements using the system shown in Figure 8. The output voltage of the transducer bridge circuit was measured by this system with the transducer driven by known diaphragm currents and gas pressures. The resulting parametric curves which were measured, fluid pressure versus output voltage and diaphragm current versus output voltage were replotted to obtain the current deflection to pressure sensitivity eliminating output voltage as a parameter. The current to pressure conversion factor measured on the breadboard transducer with the 4.25 inch wide iron diaphragm is 219 amperes/mm Hg ΔP.

The pressure versus output voltage measurement measured by this method has been discussed in detail elsewhere. The sensitivity was 1.56 mm Hg ΔP/per volt input to the PAR-HR-8 amplifier when the transducer output is connected directly to the PAR Type B preamplifier input. The

eventual projected sensitivity for this preliminary system when acoustic noise and vibration and external electrical noise are isolated from the transducer would be 1.59×10^{-9} mm Hg ΔP full scale deflection on the 10^{-9} volt range. It is apparent from this brief experimental evaluation that the effort to eliminate stray vibration, acoustic and electrical noise pickup by the transducer is a most important experimental effort to be completed. Completion of this work to reduce external noise disturbances will be an important contributing factor in demonstrating an ultimate pressure sensitivity of 10^{-8} to 10^{-9} torr.

IV

CONCLUSIONS AND RECOMMENDATIONS

A breadboard pressure balancing transducer has been designed, constructed and experimentally evaluated. This transducer utilizes an electromagnetic "J x B" pressure for the restoring pressure. The restoring pressure computed on the basis of the conceptual magnetic flux density within the current conducting diaphragm was found to be inapplicable and experimental results demonstrated the magnetic field tangential to the diaphragm will give the correct restoring pressure. A detailed redesign study based on this experimental observation has resulted in the following modification and evaluation plan for the present breadboard transducer:

1. Substitute a narrow silver diaphragm in the present breadboard transducer diaphragm frame and confirm the predicted current deflection sensitivity by measurement methods described in this report.

2. When the predicted performance of the silver diaphragm substitution is confirmed by experimental demonstration, initiate a design modification on the breadboard transducer diaphragm frame to install magnetic inserts which will increase the tangential magnetic flux density and increase the current deflection sensitivity in proportion.

3. While the design effort to modify the transducer frame for increased tangential magnetic flux and current deflection sensitivity is progressing, initiate a laboratory program which will utilize the first transducer assembly with the silver diaphragm to eliminate external acoustic, vibration and electrical disturbances which prevent achieving the 1.56×10^{-9} mm Hg ΔP full scale deflection sensitivity with the PAR – HR-8 amplifier and the type B preamplifier.

4. When the results of Step 3 have reduced the external noise due to the causes cited or progress is assured on external noise reduction, initiate construction of the transducer frame modification with magnetic inserts.

5. Demonstrate the performance of the breadboard transducer with the magnetic inserts.

6. When a satisfactory demonstration of the transducer with magnetic inserts is completed, initiate a material and design study for construction of a modified transducer with magnetic inserts, and the narrow silver diaphragm which will operate at frame temperatures from -195°C to +250°C. Preliminary computations indicate these design conditions may be satisfied with available materials.

7. Continue the development and design effort on the electronic system and installation requirements to obtain the design objective ΔP sensitivity of 10^{-8} mm Hg at low ambient pressure or 10^{-8} torr absolute pressure.

8. These steps if all accomplished should form a solid design basis
for the final prototype transducer construction and the test chamber pres-
sure meter design. The prototype transducer construction plan (which may
be the modified breadboard transducer) can be established and the detailed
electronic control system requirements can be defined in detail based on
an extensive experimental demonstration.

V

APPENDICES

The following analyses and computations are a study representing design conditions similar to the breadboard model requirements and contributed to the design of the breadboard model.

APPENDIX A

ILLUSTRATIVE TRANSDUCER THERMAL ANALYSIS

The following analyses and computations were a study representing conditions similar to those selected for the breadboard model to aid in making design choices for the breadboard model. The assumptions are:

    a. The diaphragm material is isotropic

    b. The frame temperature is approximately 0°C. This is acceptable since a typical operating temperature is 270°K to 300°K.

    c. The maximum operating pressure difference and absolute pressure is 1 torr.

    d. The peripheral temperature of the diaphragm is clamped at 0°C.

This is justified as follows:

The diaphragm is clamped between the blocks and is electrically insulated with 0.002 inch of high temperature organic film. Assume thermal conductivity of the insulator = 0.007 watt/°C/in., then

$$\frac{\Delta T}{q} = \frac{\Delta x}{KA} = \frac{2}{1000} \times \frac{1000}{7} \times \frac{1}{13} = 0.02°C/watt$$

where ΔT is the temperature difference across the insulator, the area $A = 4 \times 4 - \pi \approx 13$ in^2 (Figure 16), and q is the total heat flowing through the insulator.

Power dissipation in the diaphragm at 1 mm of Hg pressure (1 torr)

$$\approx \rho J^2 \, At$$

$$\approx \left(1700 \, \frac{amp}{in^2}\right)^2 \left(\frac{26 \times 10^{-6}}{2.54} \times ohm \, in.\right) \left(16 \, in^2\right) \left(\frac{1}{1000}\right) in.$$

$$= 0.475 \, watt$$

$$\therefore \Delta T \approx (0.475) \ (0.02) \approx 0.01°C.$$

This temperature gradient is negligible, and the temperature at the diaphragm boundary can be considered clamped to the temperature of the supporting frame.

The heat generated in the diaphragm per unit volume due to the current flow is $J^2 \rho$, where J is the current density and ρ is the electrical resistivity of the diaphragm material.

The heat is transferred from the diaphragm surface to the housing adjacent environments by conduction and radiation.

The heat conducted by low pressure gases (less than one torr) is:[20]

$$q_c = \lambda \Delta TP \ \frac{watts}{cm^2} \qquad\qquad Eq \ (25)$$

where: λ = free molecular heat conductivity

ΔT = temperature difference between diaphragm and the gas temperatures

P = pressure

The radiation term is determined as follows for parallel infinite planes:

Heat absorbed or radiated per unit area, A, is

$$q_R = 2 \left[E_1 - E_2 \right] \frac{e_1 \ e_2}{e_1 + e_2 - e_1 e_2} = 2 \left[E_1 - E_2 \right] e \qquad Eq \cdot (26)$$

where E_1 and E_2 are the terms in the Stefan-Boltzman equation of radiation heat transfer and e_1 and e_2 are the thermal emissivities of the diaphragm and the housing. The factor 2 accounts for radiation from both sides of the diaphragm.

Radiation heat transfer is obtained from the following equation[21]

$$\left[E_1 - E_2\right] = \frac{5.7}{10^{12}} \left[T_1{}^4 - T_2{}^4\right] \text{watts/cm}^2$$

It is reasonable to assume that the difference in temperatures T_1 and T_2 are small since they are given in degrees Kelvin in Equation (A-2). Neglecting higher order terms in the Binomial expansion of $(T_2 + \Delta T)^4$ where $\Delta T = (T_1 - T_2)$, we have

$$T_1{}^4 - T_2{}^4 = (T_2 + \Delta T)^4 - T_2{}^4 \approx 4 \Delta T \, T_2{}^3$$

Therefore the radiation heat transfer is:

$$q_R = \frac{5.7}{10^{12}} \text{ e } [4 \Delta T] \, T_2{}^3$$
$$; \Delta T \ll T_2$$
$$= \frac{2.27}{10^{11}} \, T_2{}^3 \text{ e } \Delta T \text{ watts/cm}^2$$

The combined heat transfer due to radiation and gaseous conduction is:

$$q = q_c + q_R = \lambda \Delta T + \frac{2.27}{10^{11}} \, T_2{}^3 \text{ e } \Delta T$$

Since $T_2 = 0°C = 273°K$ we have, $\Delta T = T°C$

$$\therefore q = \left[\lambda + \frac{4.6}{10^4} \text{ e}\right] T \text{ -------------; } T_2 = 273°K \qquad \text{Eq (27)}$$

where λ is the molecular thermal conductivity at 0°C and 1 mm Hg pressure and $e = e_1 e_2 / e_1 + e_2 - e_1 e_2$ is the combined emissivity of the diaphragm and the housing.

The time rate of change in the heat capacity of a volume element is:

$$\left(C\delta \frac{\partial T}{\partial \tau} \right) \Delta x \, \Delta yt$$

where τ is the time, C is the specific heat, δ is the mass density and T is the thickness.

Using the Fourier heat conduction law[21], the generalized heat conduction equation incorporating terms discussed previously, is given by the following equation:

$$\left(C\delta \frac{\partial T}{\partial \tau} \right) \Delta x \, \Delta yt \; = \; (\nabla^2 T) \, \Delta x \, \Delta yt + (J^2 \rho) \, \Delta x \, \Delta yt - q \, \Delta x \, \Delta y$$

Dividing both sides of the equation by $\Delta x \, \Delta yt$ we have

$$C \frac{\partial T}{\partial \tau} \; = \; k \nabla^2 T \; + \; J^2 \rho \; - \frac{q}{t} \qquad\qquad \text{Eq (28)}$$

Under steady state conditions $\dfrac{\partial T}{\partial \tau} = 0$

$$\therefore \nabla^2 T + \frac{J^2 \rho}{k} \; = \; \frac{q}{tk} \qquad\qquad \text{Eq (29)}$$

where: T = temperature in degrees centigrade

J = electric current density in the diaphragm in amps/cm^2

ρ = electrical resistivity of the diaphragm material in ohm-cm

k = thermal conductivity of the diaphragm material in watts/cm°C

t = thickness of the diaphragm in cm

q = heat transfer in watts/cm^2 and is given by Equation (25)

For different materials $\dfrac{J^2 \rho}{k}$ is computed in Table IV.

TABLE IV

$\frac{J^2\rho}{k}$ Computations for Different Materials

Restoring Pressure = 1 Torr, J = 1700 Amps/in^2

Diaphragm Thickness = 0.001 inch

Material	k $\frac{watts}{meter\ ^\circ C}$	ρ ohm-meters	$J^2\rho/k$ $^\circ$C/meter^2
Supermendur	14	26×10^{-8}	13×10^4
Pure Iron	73	10.1×10^{-8}	0.98×10^4
Low Si Steel (Si < 1%)	52	17.8×10^{-8}	2.4×10^4
Silver (99.9% pure)	410	1.63×10^{-8}	0.028×10^4

Equation (29) in radial coordinates is:

$$\frac{d^2T}{dr^2} + \frac{1}{r}\frac{dT}{dr} + \frac{J^2\rho}{k} = \frac{q}{tk} \qquad \text{Eq (30)}$$

Since q is a function of the free molecular conductivity λ, a particular equivalent gas whose value of λ is known can be used in the computation, λ of several gases at 0°C and 1 torr pressure are given in Table V.[21]

TABLE V

Gas	watts/cm^2 °C at 1 Torr	Approximate Temperature Rise in degrees centigrade at 1 mm of Hg
H_2	60.72	0.076°C
He	29.35	0.158°C
H_2O	26.49	0.171°C
Ne	13.07	0.355°C
N_2	16.63	0.278°C
O_2	15.57	0.296°C
CO_2	16.96	0.273°C
Hg	4.15	1.18°C

Referring to Figure 16 , the discretized equation at nth node is:[22]

$$\frac{(T_{n+1} + T_{n-1} - 2T_n)}{\Delta r^2} + \frac{1}{nr} \frac{T_{n-1} - T_{n+1}}{2\Delta r} + \frac{J^2 \rho}{k} = \frac{q}{tk} \quad \cdots$$
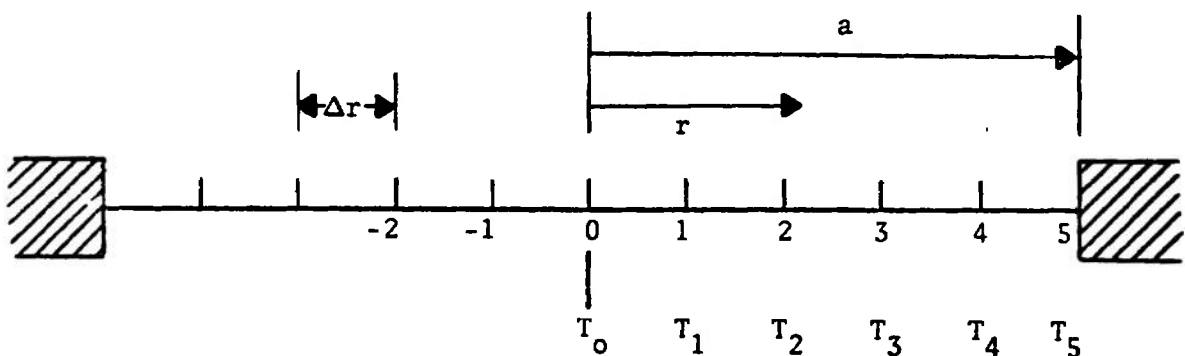
Figure 16. Discrete Temperature Locations on a Diaphragm.

Letting r = 1 cm and using Equation 25 to eliminate q, we have

$$(T_{n+1} + T_{n-1} - 2T_n) + \frac{1}{2n}(T_{n-1} - T_{n+1}) + \frac{J^2 \rho}{k} = \left(\lambda + \frac{4.6}{10^4}e\right)\frac{T_n}{tk} \quad \text{Eq (31)}$$

The Diaphragm material is Supermendur, with a bright metallic protective finish, possibly gold.

Emissivities - e_1, e_2 ------------- 0.2

- e ----------------- 0.1

Molecular gas conductivity λ_0 at 1 mm of Hg pressure for air - 16.5×10^{-3} watts/cm^2 °C.

Diaphragm thickness t ------------ $\frac{2.54}{1000}$ cm

K for Supermendur ----------------- 14 $\frac{\text{watts}}{\text{meter °C}}$

$\frac{\rho J^2}{k}$ in °C/cm^2 -------------------- 13

Equation 30 is rewritten as follows:

$$T_{n+1} + T_{n-1} - 2T_n + \frac{1}{2n}(T_{n-1} - T_{n+1}) + 13 = 46.5\, T_n$$

$$\therefore 48.5\, T_n = \left(T_{n-1} - \frac{T_{n+1}}{2n}\right) + T_{n-1}\left(1 + \frac{1}{2n}\right) + 13$$

$$\therefore 48.5\, T_n = T_{n+1}\frac{(2n - 1)}{2n} + T_{n-1}\frac{(2n + 1)}{2n} + 13$$

Boundary condition is $T_5 = 0$°C.

Using an iterative technique for n = 5, following values of temperatures in degrees centigrade are obtained:

T_0	T_2	T_3	T_4	T_5
0.277	0.2778	0.2787	0.274	0

For heavier gases such as mercury vapor λ_o is much smaller than that of nitrogen. For mercury vapor

$$\lambda_o = \frac{4}{10^3} \frac{watts}{0° \ cm^2} \quad at \ 1 \ torr$$

The discretized equation is:

$$13 \ T_n = T_{n+1} \frac{(2n+1)}{2n} + T_{n-1} \frac{(2n+1)}{2n} + 13$$

The equation is solved for n = 5 by iterative technique and the solution is shown below in degrees centigrade:

T_0	T_1	T_2	T_3	T_4
1.18	1.176	1.176	1.170	1.096

For light gases such as hydrogen, heat transfer to the diaphragm is more efficient than in the case of a heavier gas such as mercury vapor.
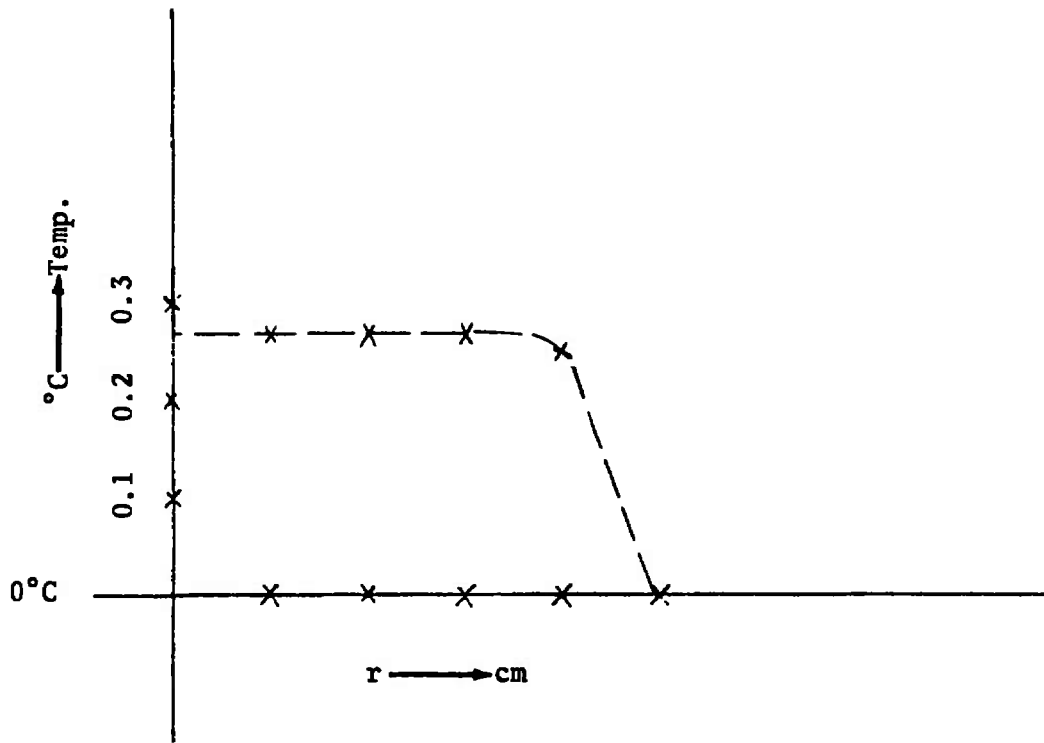
Figure 17.   Plot of Diaphragm Temperature Vs. Radius For
Gaseous Nitrogen at 0°C and 1 Torr Pressure
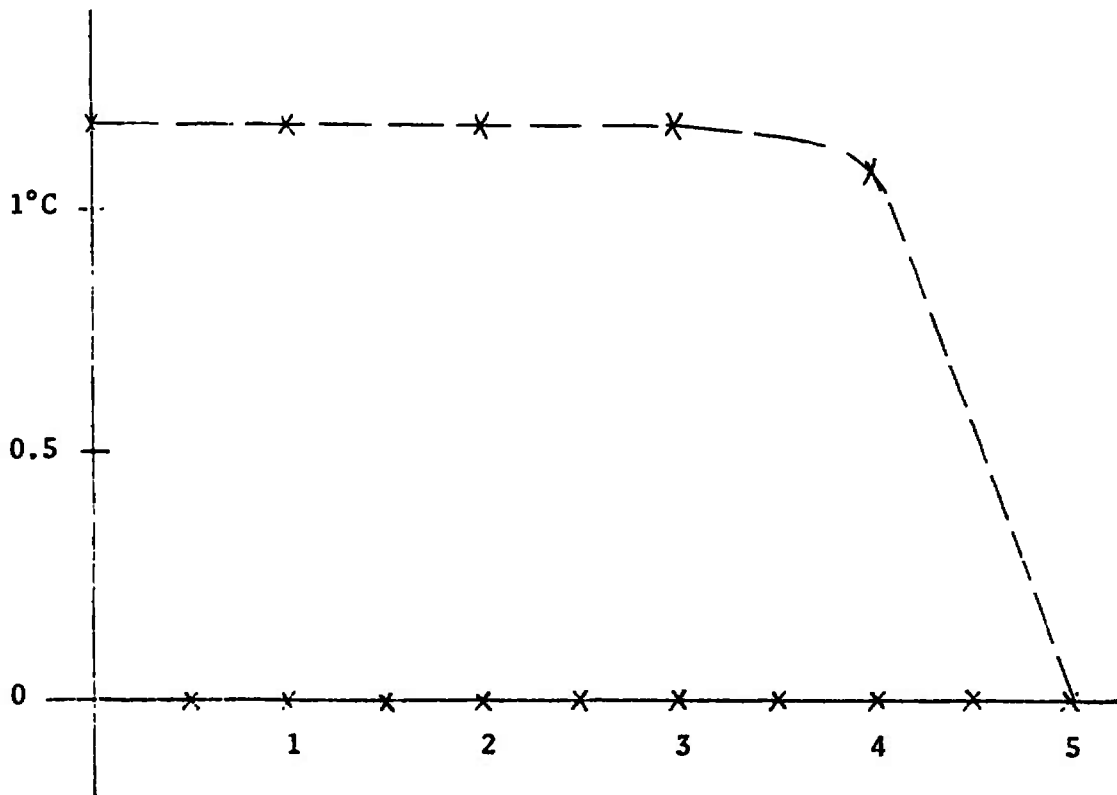
Figure 18.   Diaphragm Temperature Vs. Radius For Mercury
Vapor at 1 Torr Pressure

For other gases, maximum approximate temperature rise of the diaphragm is given in Table VI. For most common gases the temperature rise will be less than 0.5°C. The temperature rise can be further reduced by using a diaphragm material of higher electrical and/or thermal conductivity such as pure iron or silver (see Table IV.). The temperature rise considered here for different gases is at the upper measurement limit of the differential pressure, for absolute zero reference pressure. For pressures lower than 1 torr, the temperature rise will be lower.

The order of magnitude of error in the solution of discretized equation is obtained from Tailor's series.

$$\epsilon_1 = \frac{\Delta r}{2r} \frac{\partial^2 T}{\partial^2 r} \quad \text{for 1st derivative term}$$

For mercury vapor, at $r = 4$,

$$\epsilon_1 = \frac{1}{8} [T_3 - 2T_n]$$

$$= \frac{1}{8} [1.17 - 2.192]$$

$$= 0.127°C$$

$$\therefore \% \text{ error in } \Delta = \frac{12.7}{1.17} \approx 11\%$$

TABLE VI

Approximate Temperature Rise of Diaphragm above the Frame Temperature at Low Pressures

Pressure in Torr	1	10^{-1}	10^{-2}	10^{-3}	10^{-4}	10^{-5}	10^{-6}	10^{-7}
$J^2\rho/k$ °C/cm^2	13	0.13	13×10^{-4}	13×10^{-6}	13×10^{-8}	13×10^{-10}	13×10^{-12}	13×10^{-14}
$1000\,\lambda$ watts/ cm^2 for air	16.5	1.65	.165	16.5×10^{-3}	16.5×10^{-4}	16.5×10^{-5}	16.5×10^{-6}	16.5×10^{-7}
q/tk	46.5	4.8	0.58	0.1765	0.134	0.130	0.130	0.130
Approx $\Delta T = \dfrac{J^2\rho/k}{q/tk}$	0.278	0.027	2.25×10^{-3}	7.4×10^{-5}	9.7×10^{-7}	10^{-9}	10^{-11}	10^{-13}

APPENDIX B

TRANSDUCER TEMPERATURE TRANSIENT EFFECTS

The thermal capacity of the diaphragm acts analogous to a capacitor charging from a constant resistance and voltage. The constant resistance heat supply corresponds to the gas temperature differential near the diaphragm surface. The time constant of the thermal transient effect is:

$$\delta C \, \pi a^2 t \, \frac{dT}{d\tau} = + \lambda A \, (T_g - T) \qquad \text{Eq (32)}$$

where: T = temperatures of the diaphragm

δ = the density of the diaphragm material

C = thermal capacity of the diaphragm

a = radius

t = thickness of the diaphragm

τ = time

T_g = gas temperature

Let $(T_g - T) = \Theta$.

$$\therefore \delta C \, \pi R^2 t \, \frac{d\Theta}{d\tau} = \lambda A \Theta$$

or

$$\frac{d\Theta}{\Theta} = - \frac{\lambda A}{\delta C \pi R^2 t} \, d\tau = - \beta d\tau$$

Integrating both sides we have

$$\Theta = \Theta_o \, e^{-\beta\tau} \qquad \text{Eq (33)}$$

when $1/\beta$ is the time constant.

For nitrogen gas at 0°C and 1 torr, the time constant is:

$$1/\beta = \frac{\delta C \pi R^2 t}{\lambda \pi R^2} \qquad\qquad \text{Eq (34)}$$

$$= \frac{8.3 \times 0.46 \times 2.54}{16.5} = 0.59 \text{ sec.}$$

Note that λ includes radiation transfer at low pressures. The radiation transfer assumes the parallel plane condition (shape factor = 1).

For mercury vapor at 0°C and 1 torr, the time constant is:

$$1/\beta = 0.59 \times \frac{16.5}{4.15} = 2.35 \text{ seconds.}$$

The time constants of various gases at different pressures are computed disregarding the heat conduction from the diaphragm to the frame (Table VII). Note that at pressures higher than 10^{-2} torr, the molecular gas conduction predominates; at pressures lower than 10^{-4} torr, the radiation predominates.

If the conduction from the diaphragm to the frame is considered, an approximate electrical analog of the heat flow is shown in Figure 19.
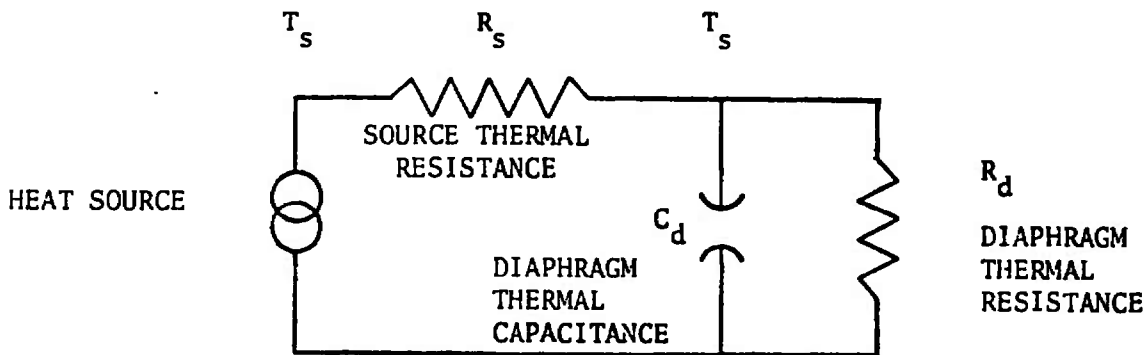

Figure 19. Electrical Analog of Diaphragm Heat Conduction.

TABLE VII

Time constants of gases at different pressures assuming that
the heat conduction from diaphragm to frame is very small

Gas	Pressure in Torr								
	1.0	10^{-1}	10^{-2}	10^{-3}	10^{-4}	10^{-5}	10^{-6}	10^{-7}	10^{-8}
H_2	0.160	1.59	14.8	86	187	208	211	211	211
He	0.333	3.27	28.7	130	200	210	211	211	211
H_2O	0.367	3.60	31.2	134	200	209	211	211	211
Ne	0.745	7.25	55	165	207	211	211	211	211
N_2	0.585	5.70	45.5	157	205	211	211	211	211
O_2	0.628	6.11	46.5	158	206	211	211	211	211
CO_2	0.575	5.60	45.5	156	205	211	211	211	211
Hg	2.35	22	113	197	212	212	212	212	212

The diaphragm thermal capacitance is:

$$C_d = \delta \pi a^2 tc = \frac{8.3 \times 71 \times 1 \times 16.4 \times .46}{1000}$$

$$= 0.196 \text{ Joule/}^\circ C$$

The time constant $(1/\beta)$ at low pressures is:

$$1/\beta = R_s C_d = 211 \text{ sec.}$$

$$\therefore R_s = \frac{211}{0.196} = 1080 \text{ }^\circ C/\text{watt}$$

The approximate diaphragm thermal resistance R_d computations using the discretized technique similar to the one used in Appendix A is $1100^\circ C/\text{watt}$.

Therefore, the maximum thermal time constant of the diaphragm is approximately 105 seconds at pressures lower than 10^{-4} Torr.

Under steady state conditions the temperature of the diaphragm is:

$$T_d = \frac{R_d}{R_s + R_d} T_s \qquad\qquad \text{Eq (35)}$$

The value of R_s is computed based on the assumption that the shape factor is 1, corresponding to infinite parallel plane heat transfer boundaries.

The shape factor for typical geometries which may exist in the orbital test chamber application will be much less than 1. This will greatly reduce the steady state temperature rise of the diaphragm.

VI

REFERENCES

1. <u>Electromagnetics</u>, J. D. Kraus, McGraw-Hill Book Co., 1953.

2. Pressure Gauge with Diaphragm Null Position Means, O. O. Fiet, United States Patent No. 3,529,238, September 15, 1970.

3. <u>Ultra-Vac Differential Pressure Gauge</u>, TRW Systems Group Proposal 12109.000, 15 August 1968, to Headquarters - Arnold Environmental Development Center, Arnold Air Force Station, Tullahoma, Tennessee.

4. <u>Permanent Magnets and Their Application</u>, R. J. Parker and R. J. Studders, John Wiley & Sons, Inc., New York, 1962.

5. <u>Instruction Manual for MKS Baratron Type 77 Electronic Pressure Meter</u>, MKS Instruments Inc., 45 Middlesex Turnpike, Burlington, Mass.

6. "Instruction Manual for Precision Lock-In Amplifier Model HR-8," Princeton Applied Research Corporation, Princeton, N.J., 1969.

7. <u>Network Analysis and Feedback Amplifier Design</u>, H. W. Bode, D. Vr.1 Nostrand Co. Inc., New York, 1945.

8. <u>Radio Engineers Handbook</u>, F. E. Terman, First Edition, McGraw-Hill Book Co., 1943.

9. <u>Formula for Stress and Strain</u>, R. J. Roark, 3rd Edition, McGraw-Hill Book Co.

10. "Fluctuation Theory in Physical Measurements," C. W. McCombie, <u>Rep. Progr. Physics</u>, 16, 266 (1953).

11. <u>A Textbook of Sound</u>, A. B. Wood, Bell & Sons, 1957.

12. <u>Vibration and Sound</u>, Morse, McGraw-Hill Book Co., 1948

13. <u>Acoustics</u>, L. L. Beranek, McGraw-Hill Book Co., 1954

14. <u>Aerospace Structural Materials Handbook</u>, Vol. I, Supplement I, Ferrous Alloys, Syracuse University Press, 1968, AFML-TR-68-115.

15. <u>W.A.D.D. Technical Repoi" 60-56</u>, Part II.

16. <u>Ferromagnetism</u>, R. M. Bozorth, D. Van Nostrand Co. Irc., New York, 1955.

17. "Properties of High Purity Iron," H. E. Cleaves & J. M. Hiegal, <u>Jour. Res. Nat. Bur. Stds.</u>, 28, 643-67.

18. "Investigation of Thermal Expansion of Some Metals and Alloys with an Improved Dilatometer," H. Esser, et al, <u>Arch. Eisenhüttenw</u>, 14, 341-55, 53.

65

19. <u>1971 Materials Engineering Materials Selector</u>, Reinhold Publishing Corp., Stamford, Conn., Nov. 1970, Vol. 72, No. 6.

20. <u>Scientific Foundations of Vacuum Technique</u>, S. Dushman and Lafferty, John Wiley & Sons, 2nd Edition.

21. <u>Heat and Mass Transfer</u>, Eckert & Drake, 2nd Edition, McGraw-Hill Book Co.

22. <u>Analog Simulation</u>, W. J. Karplus.

DOCUMENT CONTROL DATA - R & D

(Security classification of title, body of abstract and indexing annotation must be entered when the overall report is classified)

1. ORIGINATING ACTIVITY *(Corporate author)*	2a. REPORT SECURITY CLASSIFICATION
TRW Systems Group Redondo Beach, California 90278	UNCLASSIFIED
	2b. GROUP N/A

3. REPORT TITLE

RESEARCH AND DEVELOPMENT OF A TRANSDUCER FOR TEST CHAMBER MEASUREMENT

4. DESCRIPTIVE NOTES *(Type of report and inclusive dates)*

Final Report - 1 July 1969 to 30 April 1971

5. AUTHOR(S) *(First name, middle initial, last name)*

Owen O. Fiet

6. REPORT DATE	7a. TOTAL NO OF PAGES	7b. NO. OF REFS
December 1971	73	22

8a. CONTRACT OR GRANT NO. F40600-69-C-0009	9a. ORIGINATOR'S REPORT NUMBER(S)
b. PROJECT NO. 4344	AEDC-TR-71-144
c. Program Element 65701F	9b. OTHER REPORT NO(S) *(Any other numbers that may be assigned this report)*
d. Task 37	N/A

10. DISTRIBUTION STATEMENT

Approved for public release; distribution unlimited.

11. SUPPLEMENTARY NOTES	12. SPONSORING MILITARY ACTIVITY
Available in DDC	Arnold Engineering Development Center Air Force Systems Command Arnold Air Force Station, Tennessee 37389.

13. ABSTRACT This report describes the initial design, construction and development of a diaphragm type pressure balancing transducer which uses the electromagnetic "J x B" force to balance the applied fluid pressure. The pressure is measured by the direct substitution of electromagnetic pressure and a measurement of the current required to produce the balancing pressure. This technique for pressure measurement results in a direct pressure measurement by substitution and is independent of the tension and elastic constants of the pressure sensing diaphragm provided positive tension is sustained in the diaphragm. Experimental measurements on the breadboard model demonstrate the magnetic field tangential to the diaphragm should be used in calculating the restoring pressure due to diaphragm current flow. Recommendations for design improvements on the breadboard transducer are made which are intended to obtain a transducer to operate from -195°C to +250°C. These improvements accompanied by a development effort to reduce external vibration, acoustic and electrical disturbances (electronic system and installation practices) are expected to enable demonstration of pressure measurements to 10^{-8} torr using adaptations of available commercial laboratory equipment. The development of this type of pressure transducer is important for orbital rocket engine test chamber pressure measurements because it will enable fundamental direct physical pressure measurement (force per unit area) at low pressures independent of gas species. Results projected from experimental work completed on the breadboard model confirm earlier predictions that the performance goals for a temperature range of -195°C to +250°C and sensitivity to 10^{-8} torr may be obtained.

DD FORM **1473**
I NOV 65

14. KEY WORDS	LINK A		LINK B		LINK C	
	ROLE	WT	ROLE	WT	ROLE	WT
pressure sensors						
breadboard models						
design						
construction						
performance						
rocket exhausts						
measurements						

AFSC
Arnold AFB Tenn